EBioMedicine 45 (2019) 108–123

Contents lists available at ScienceDirect

EBioMedicine

journal homepage: www.ebiomedicine.com

EBioMedicine
Published by THE LANCET

Research paper

Fatty-acid receptor CD36 functions as a hydrogen sulfide-targeted receptor with its Cys333-Cys272 disulfide bond serving as a specific molecular switch to accelerate gastric cancer metastasis

Rui Wang [a,1], Beibei Tao [b,1], Qilin Fan [c], Shengyue Wang [a], Li Chen [d], Junjie Zhang [a], Yinfang Hao [a], Shuang Dong [a], Zhe Wang [a], Wei Wang [a], Yixi Cai [e], Xutong Li [f], Tuvshin Bao [g], Xiaohui Wang [h], Xiaoming Qiu [i], Kekun Wang [j], Xinyu Mo [k], Yuqi Kang [l], Zhirong Wang [a,*]

[a] Department of Gastroenterology, Tongji Hospital, Affiliated to Tongji University, Shanghai 200065, China
[b] Department of Physiology and Pathophysiology, School of Basic Medicine, Fudan University, Shanghai 200032, China
[c] Cancer Center, Union Hospital, Tongji Medical College, Huazhong University of Science and Technology, Wuhan 430030, China
[d] Department of Gastroenterology, Baoshan Branch, Renji Hospital, Affiliated to Shanghai Jiaotong University, Shanghai 200444, China
[e] Department of Pediatrics, First People's Hospital of Liangjiang New District, Chongqing 401121, China
[f] Department of Neurology, Minhang Branch, Zhongshan Hospital, Fudan University, Shanghai 200032, China
[g] Department of Anesthesia, Union Hospital, Tongji Medical College, Huazhong University of Science and Technology, Wuhan 430030, China
[h] Department of Pancreatic Surgery, State Key Laboratory of Oncology in South China, Zhongshan University, Guangzhou 510001, China
[i] Department of Orthopedics, Provincial Hospital of Gansu Province, Lanzhou 730001, China
[j] School of Health Science, Wuhan University, Wuhan 430030, China
[k] First Teaching Hospital of Tianjin University of Traditional Chinese Medicine, Tianjin 300001, China
[l] Department of Oncology, Oncology Hospital of Guizhou Province, Guiyang 550001, China

ARTICLE INFO

Article history:
Received 15 February 2019
Received in revised form 12 June 2019
Accepted 19 June 2019
Available online 28 June 2019

Keywords:
H_2S
CD36
Disulfide bond
Long chain-fatty acid
Nrf2
Metastasis

ABSTRACT

Background: Hydrogen Sulfide (H_2S), a third member of gasotransmitter family along with nitric oxide (NO) and carbon monoxide (CO), exerts a wide range of cellular and molecular actions in our body. There is a large body of evidence suggesting that H_2S plays an important role in cancer metastasis; however, the molecular mechanisms of H_2S-mediated acceleration of cancer metastasis remain unknown.
Methods: We examined the promote effects of H_2S on phenotype of gastric cancer (GC) cells (including those of express wild type CD36 and mutant CD36) *in vitro* and *in vivo*. GC patients' samples were used for clinical translational significance evaluation.
Findings: H_2S triggered lipid metabolism reprogramming by significantly up-regulating the expression of the fatty-acid receptor CD36 (CD36) and directly activating CD36 in GC cells. Mechanistically, a disulfide bond located between cysteine (Cys)333 and Cys272 within the CD36 protein structure that was labile to H_2S-mediated modification. The long chain-fatty acid (LC-FA) binding pocket was capped by a turn in the CD36 protein, located between helical and sheet structures that were stabilized by the Cys333-Cys272. This limited the secondary binding between LC-FAs and lysine (Lys)334. Breaking the Cys333-Cys272 disulfide bond restored the second LC-FA binding conformation of CD36. Targeting CD36 *in vivo* blocked H_2S-promoted metastasis and improved animal survival.
Interpretation: These findings identify that the Cys333-Cys272 disulfide bond disrupted the integrity of the second LC-FA binding conformation of CD36. Therefore, CD36 can directly activate LC-FA access to the cytoplasm by acting as a direct target molecule for H_2S.

1. Introduction

H_2S, a third member of gasotransmitter family along with NO and CO, exerts a wide range of cellular and molecular actions in our body [1–3]. While H_2S at high concentrations is toxic, low levels impart numerous benefits [4–8]. H_2S is produced endogenously by several

* Corresponding author at: Department of Gastroenterology, Tongji Hospital Affiliated to Tongji University, Shanghai 200065, China.
E-mail address: wangzr_tongji@163.com (Z. Wang).
[1] These authors contributed equally.

https://doi.org/10.1016/j.ebiom.2019.06.037

Research in context

Evidence before this study

GC is a silent disease that is often diagnosed at late stages leading to poor patient survival. Metabolism alterations are hallmarks of cancer, but the involvement of lipid metabolism in disease progression is unclear. H_2S, a third member of gasotransmitter family along with NO and CO, exerts a wide range of cellular and molecular actions in our body. There is a large body of evidence suggesting that tumor-derived H_2S, which is produced endogenously by several enzymes, stimulates bioenergetics, induces angiogenesis, and accelerates metastasis in cancer; however, the molecular mechanisms of H_2S-mediated acceleration of cancer metastasis remain unknown.

Added value of this study

The present study provides the evidence for H_2S-targeted receptor and reveals a new intrinsic inhibitory S—S bond in CD36 that serves as a molecular switch for H_2S-induced modification and factional regulation. Expression of mutant CD36(C333A) promoted metastasis of GC cells and prevented the enhancing effect of H_2S *in vivo*. Endogenous H_2S was also necessary for CD36-induced, antiangiogenic drug resistance.

Implications of all the available evidence

These findings identify a critical role for H_2S-mediated acceleration of GC metastasis and suggest that targeting CD36-mediated LC-FA uptake has therapeutic effects in preclinical models of GC metastasis. Our study provides new insights for a better understanding of the molecular mechanisms of H_2S in cancer metastasis.

enzymes, including 3-mercaptopyruvate-sulfurtransferase (3MST), cystathionine-β-synthase (CBS), and cystathionine-γ-lyase (CSE) [9–11]. Recently, an increasing number of studies have reported the significantly increased expression of various H_2S-producing enzymes in cancer cells of diverse tissue types, and new roles of H_2S in the pathophysiology of cancer have emerged [12]. Although extremely limited in terms of mechanistic detail, there is a reasonable body of evidence suggesting that H_2S plays an important role in cancer metastasis [13,14].

The metabolic reprogramming of cancer cells has been established as a hallmark of cancers, where the rate of mitochondrial adenosine-triphosphate (ATP) production, but not glycolytic ATP production inversely correlates with cancer-cell doubling time. Glycolysis is not a major contributor of total ATP but allows nutrient assimilation into biosynthetic precursors [15]. Therefore, highly metastatic cancer cells exhibit avid lipid metabolism, which they compensate for by increasing lipid uptake from exogenous sources [16].

CD36 is a scavenger receptor whose primary function is the high-affinity uptake of long-chain fatty acids (LC-FAs) [17]. Increasing evidence indicates the existence of specific cells called metastasis-initiating cells (MICs), which may originate from a heterogeneous population of cancer cells in the primary tumor but then continue to evolve during dissemination and colonization [18]. A recent study showed that CD36-dependent lipid metabolism was an important component of metabolic reprogramming for cancer cell metastasis but not primary cancer cell growth, which suggested a unique requirement for lipid metabolism reprogramming in initiating cancer cell metastasis [18,19]. As the most energy-efficient way to generate ATP to satisfy the energy requirements of cancer cell metastasis, lipid metabolism is perhaps particularly crucial for the metastasis of disseminated cancer cells in a new microenvironment [20]. Both a high-fat diet and adipocyte-conditioned media were found to increase the percentage of CD36-positive cancer cells and to promote metastasis [18]. Clinically, obesity has also been linked to an increased risk of metastasis in breast cancer [21]. These findings establish CD36 as a marker and functional driver of cancer cell metastasis *via* its function in lipid metabolism. CD36 has been associated with tumor progression and poor prognosis in glioblastoma cancer [22]. While many details have yet to be investigated, the identification of CD36 as a MIC marker expands our knowledge of lipid metabolism in cancer progression and adds a promising new target for the development of anti-metastasis therapeutic strategies [23–25].

Cancer cells are also hallmarked by high proliferation and imbalanced redox consumption and signaling [26]. Various oncogenic pathways such as proliferation and evading cell death converge on redox-dependent signaling processes [27]. Nrf2 is a key regulator in these redox-dependent events and operates in cytoprotection, drug metabolism and malignant progression in cancer cells [28,29].

Metabolism alterations are hallmarks of GC, but the involvement of lipid metabolism in disease progression is unclear. We investigated the role of lipid metabolism in GC using cell-derived xenograft mouse models. We showed that LC-FA uptake was increased in GC cells and that these LC-FA directed toward biomass production. These changes were mediated, by the fatty acid transporter CD36, which was associated with aggressive disease.

The fact that the mechanism of H_2S-mediated acceleration of cancer metastasis is unknown hampers the development of anti-metastasis therapies. In this study, we found that CD36 functioned as a H_2S-targeted receptor. Its Cys333-Cys272 disulfide bond served as a specific molecular switch that activated the LC-FA binding conformation of CD36, thereby promoting LC-FA uptake and accelerating the spread of GC. The use of neutralizing antibodies or inhibitors to block CD36 could accomplish an almost complete inhibition of metastasis in immunodeficient orthotopic mouse models of oral squamous cell carcinoma, with no side effects [25,30].

2. Materials and methods

2.1. Cell culture

The human GC cells (AGS, HGC27, NCI-N87, and KATO III) were purchased from ATCC (Manasseh's, VA, USA). The human GC cells (SGC7901, MGC803, MKN45) and human gastric epithelial cells (GES-1) were obtained from the Institute of Tongji Hospital Affiliated to Tongji University. Cells were cultured in RPMI1640 (Gibco, USA) supplemented with 10% Foetal Bovine Serum (FBS) (Gibco, USA), 1% penicillin-streptomycin (PS) and 1% nonessential amino acids in a humidified, 5% CO_2 air atmosphere at 37 °C. Cell lines were characterized by gene sky biopharma technology using Short Tandem Repeat (STR) markers.

2.2. RNA-sequencing (RNA-seq) and real-time quantitative PCR

For the mRNA-seq assay, samples were submitted to Shanghai Majorbio Bio-pharm Technology Corporation for RNA-seq. Poly (A) RNA was purified from total RNA, then converted to double-stranded cDNA; the resulting cDNA samples were sequenced using the standard Solexa protocols. The sequencing reads were mapped to the human genome using tophat. Avadis NGS was used to calculate reads per kilobase per million mapped reads (RPKM) values. Differentially expressed genes were called at two-fold changes using RPKM. Gene ontology (GO) enrichment and Kyoto Encyclopedia of Grene and Genomes (KEGG) pathway analyses were performed with DAVID (Database for Annotation, Visualization and Integrated Discovery). For real-time PCR, total RNA was isolated using Trizol reagent (Invitrogen), then cDNA was generated by reverse transcription of aliquots of RNA

using the Takara PrimeScript RT Reagent Kit (Takara) according to the manufacturer's instruction. The resulting cDNA was used for real-time PCR with SYBR® Premix Ex Taq™ Kit (Takara) in a StepOne Real-Time PCR Detection System (Life Technologies). All expression data were normalized to GAPDH-encoding transcript levels. Primers used for real-time PCR are shown in Supplementary Table Information. The RNA-seq data has been deposited to National Center for Biotechnology Information (NCBI) *via* the Sequence Read Archive (SRA) database repository with the dataset identifier (Study SRA BioProject accession number No.: PRJNA548275).

2.3. Metabolic assay

Mitochondrial oxygen consumption rate (OCR), extracellular acidification rate (ECAR), fatty acid oxygen (FAO), ATP production was conducted using a seahorse real-time bioenergetics analyzer (Agilent Bioscience) for metabolic assay. The GC cells were seeded into XFp microplates and cultured at 37 °C with 5% CO_2. The following day, the media was replaced with 700 μl assay medium composed of DMEM without FBS and sodium bicarbonate and incubated at 37 °C without CO_2 for 1 h. For the glycolytic stress test (Seahorse Cat. #103020-100), 10 mM glucose, 1 μM oligomycin and 50 mM 2-deoxyglucose (2-DG) were injected to the wells. For the mitochondrial stress test (Seahorse Cat. #103015-100), 2 μg/ml oligomycin, 2.5 μM carbonylcyanide-ptrifluorometthoxyphenylhydrazone (FCCP), 0.5 μM rotenone and 2 μM antimycin A were add to the wells. Both measurements were normalized by total protein quantitation.

2.4. Spectrometry studies

Liquid chromatograph-mass spectrometer (LC-MS) analyses of model chemicals were performed using a SHIMADZU mass spectrometer (MS). CD36 was digested with trypsin and on-line isolation was performed using high-performance liquid chromatography (HPLC) (Michrom Bioresources). Sample digests were analyzed using tandem MS with an LTQ Orbitrap XL MS (Thermo Electron).

2.5. Multiple reaction monitoring (MRM) analysis

Total lipid was extracted from 2×10^7 cells, using a modified method of Bligh and Dyer. An internal standard cocktail (Avanti Lipids Polar) was added at an amount of 10 μl to each sample according to 1 mg of extracted tissue protein during lipid extraction. Lipid extracts were subjected to triple-quadrupole MS (QTRAP 4000 and 6500; SCIEX, Framingham, MA). Both negative and positive electrospray ionization modes were used, and precursor ion scans and neutral loss scans were run in each mode. Lipid identification was based on MS data and assisted by the bioinformatics tool Lipid MS Predict (http://www.lipidmaps.org/). Quantitation was done by one internal standard per lipid class. Each experiment was repeated at least three times. Lipid compositions were separated on the Shimadzu LC-20AB HPLC system (Tokyo, Japan).

2.6. Construction of human mutant CD36 (C333A), Overexpression of human mutant CD36 (C333A) and wild-type human CD36

Mutational analysis was conducted in which Cys333 was replaced with an alanine (C333A). Mutant CD36(C333A) prevent the formation of the Cys333-Cys272 disulfide band was transfected and express in GC cells using a lentivirus vector. Mutant CD36 (C333A) without the Cys333-Cys272 disulfide bond was provided by SignalChem according to a custom-development program. CD36 (NM_000072) mutated at Cys333 or wild-type CD36 was cloned into pGC-FU, the lentiviral vector expression plasmid. GC cells grown at 70%–80% confluence was infected with the mutant lentivirus, wild-type CD36 lentivirus, or control lentivirus. The cells were passaged for further experiments after infection for 3 days.

2.7. Animal study

Male BALB/c athymic nude mice (aged 4–5 weeks) were maintained in pathogen-free conditions with a 12-h light/dark cycle. This animal study was conducted in accordance with the rules and regulations of the Institutional Animal Care and Use Committee at the Department of Laboratory Animal Science, Fudan University. For the subcutaneous xenograft tumor model, AGS-Luciferase cells at a density of 5×10^6 in 0.2 mL PBS were injected subcutaneously into the legs of nude mice. For the orthotopic xenograft tumor model, AGS-Luciferase cells at a density of 1×10^6 in 0.2 mL PBS were injected into the subcutaneous serosal membrane in gastric tissue of the nude mice. Tumor volume and spontaneous distant metastases were measured with a Vernier caliper and a Xenogen IVIS 2000 Luminal Imager. After 3 weeks, the mice were killed.

2.8. RNAi-mediated knockdown of human CD36, CSE and Nrf2

Lipofectamine-mediated transient transfection of human CD36, CSE and Nrf2 small interfering RNA (siRNA) was performed. Short hairpin RNA (shRNA) directed against human CD36 was inserted into the pLKO.1 vector. 293 T cells were transiently transfected with the following plasmids: lentiviral packaging plasmid pMD2.G, psPAX2, and lentiviral expression plasmid. Forty-eight hours post-transfection, the supernatant was harvested. The sequences of siRNA and shRNA against human CD36, CSE and Nrf2 used in our studies are described in Supplementary Table Information.

2.9. Wound healing assay

Confluent human GC cells were starved overnight and were scratched using a pipette tip for the wound healing assay. Markings were drawn on the culture dishes as reference points so as to make sure that the same visual field was photographed at 0 h and 24 h. Typically, 8–12 visual fields were chosen randomly in one culture dish. Cells were photographed using an EVOS fl Microscope (Advanced Microscopy Group, Mill Creek, Washington) after incubation, according to the suppliers' instructions. The outline of the wound area (the area with no cells) was then drawn using Image J software to get the exact pixel coverage of each wound area.

2.10. Cell invasion assay

Transwell chambers (8 μm pore size; Corning Life Sciences) were coated with 100 μl of diluted Matrigel. 0.6 ml medium containing 20% FBS was added to the lower chambers, and cells suspended in serum-free medium at a density of 1.5×10^5 cells/ml were seeded (0.1 ml) in the upper chambers. Various concentrations of NaHS were added to both of the upper and lower chambers. After cultured for an appropriate time (24 h), cells were then fixed by cold 95% ethanol, stained by 0.1% crystal violet, and cells that had not migrated were removed from the upper chambers. The remaining cells were photographed. The dye was dissolved in 80 μl of 10% acetic acid, and the absorbance of the resulting solution was measured at 600 nm using a multiwall spectrophotometer.

2.11. Determination of intracellular reactive oxygen species (ROS)

2,7-dichlorofluorescin diacetate (DCFH-DA) (Sigma) was used to measure intracellular ROS levels in human GC cells was determined with staining immunofluorescence and observed using a laser scanning microscope (Leica TCS SP5).

2.12. BODIPY staining

For BODIPY staining, human GC cells were fixed with aceton for 10 min, rinsed with PBS, and then stained with BODIPY 558/568 for 15 min. Positive signals were captured using a fluorescence microscope equipped with a camera (Nikon DS-Qi1MC).

2.13. Detection of the mitochondrial membrane potential (MMP)

The MMP was measured by fluorescence microscopy using the Tetramethylrhodamine methyl ester (TMRM) probe. Fluorescent images of treated cells were acquired and fluorescence intensities were analyzed, as previously described, through a Zeiss Axiovert 200 microscope equipped with a Photometrics Cascade 512B CCD camera and using MetaFluor software.

2.14. Western blot

Cell lysates were determined with Bicinchoninic acid (BCA) method, and an equal amount of proteins was separated by SDS-PAGE and then transferred to nitrocellulose membranes. The membranes were blocked with 5% (*w*/*v*) non-fat dry milk, followed with overnight incubation at 4 °C with the following antibodies which were provided in Supplementary Table. Immunoreactive proteins were detected using ECL Plus (Thermo Fisher Scientific), after secondary antibody incubation.

2.15. 2-Deoxyglucose uptake

The GC cells were rinsed with a KRP buffer (128 mM NaCl, 4.7 mM KCl, 1.25 mM $CaCl_2$, 1.25 mM $MgSO_4$, 5 mM NaH_2PO_4, 5 mM Na_2HPO_4, and 10 mM HEPES, pH 7.4), containing 0.1% (w/v) BSA and 5 mM glucose every 40 min for a total of 120 min at 37 °C. The cells were then treated with 100 nM insulin in a KRP buffer without glucose for 15 min or left untreated. 2-deoxy-D [^{3}H]-glucose (1 $\mu Ci \cdot ml^{-1}$) was added, and the cells were incubated for 15 min. The cells were rinsed three times in ice-cold PBS containing 10 mM glucose, and they were then lysed with 0.4 nM NaOH. [^{3}H] radioactivity was measured in a liquid scintillation counter (Beckman LS6500). Each sample was measured in triplicate. Nonspecific uptake was determined in the presence of cytochalasin B (10 μM) and was subtracted from each value. A transient treatment (15 min) with 100 nM insulin in the KRP buffer before the cells were treated with radioactive glucose was applied in both the cells cultured with low glucose (5.5 mM, without insulin) and the cells cultured with high glucose (25 mM) with insulin (100 nM). In these experiments, the concentration of insulin applied in the following glucose-uptake assay (including the transient insulin treatment before application of 2-deoxy-d [^{3}H]-glucose and the insulin contained after application of 2-deoxy-D[^{3}H]-glucose) was identical to that used in the cell culture period.

2.16. Nrf2 luciferase reporter assay

Luciferase reporter assay was performed using a Dual-Luciferase Reporter Assay System (Promega). Luciferase reporters were transfected into cells cultured in 35 mm dishes with or without NaHS treatment as described.

2.17. Chromatin Immunoprecipitation (ChIP) assays

The ChIP assay was performed according to the protocol described previously. In brief, after treatment, the GC cells were treated with 1% formaldehyde for 10 min to crosslink chromatin and protein. The chromatin-protein samples were immunoprecipitated with Nrf2 antibody. The immunoprecipitates were then incubated with protein A/G agarose beads. After several washes, the protein-DNA complex was reversed. DNA was purified using phenol-chloroform. The DNA was analyzed by qPCR using primers that were specific for regions spanning the Nrf2 binding sites in the promoters of *CD36*.

2.18. Immunohistochemistry (IHC)

IHC was performed on paraffin-embedded sections of human GC (214 stomach cancer tissues). Formalin fixed, paraffin embedded consecutive human GC tissue sections (3-5 μm) were deparaffinized and rehydrated. Antigen retrieval was performed by boiling tissue sections in 10 mM citrate buffer (pH 6.0) in a microwave oven for 5 min. The activity of endogenous peroxidase was blocked with 3% hydrogen peroxide in methanol for 10 min at room temperature. After washing, non-specific binding sites were blocked by incubating the slides with 10% FBS/PBS for 30 min at room temperature. Sections were subsequently incubated with antibodies against CSE and CD36 at 4 °C overnight. After incubation with the primary antibodies, the sections were washed and incubated with secondary antibodies and DAB staining reagent with GTVision™ Detection System/Mo&Rb Kit according to manufacturer's instructions. After counterstain with hematoxylin and dehydration, the sections were mounted and imaged using the Leica microscope. The corresponding tissue array (with 214 cases and a total of 10 holes as normal control) was subjected to IHC staining for CSE and CD36 expression. Immunoreactivity was qualitatively evaluated according to the area of staining despite the intensity to avoid artificial cut-off effect: the area of stained cancer cells was recorded as 0% (negative staining), > 0% (positive staining) of all cancer cells.

2.19. Measurement of the activity of CSE and 3MST

To measure the CSE activity, the enzyme substrate L-cysteine (10 mM) and the cofactor pyridoxal-5′-phosphate (2 mM) were added to the cells for an incubation of 4 h. To measure 3MST activity, L-cysteine (5 mM) and α-ketoglutarate (1 mM) were added to the cells for an incubation of 4 h according to the methods described by Shibuya et al. who show that Cys aminotransferase generates 3-mercaptopyruvate (3MP) in the presence of Cys and a-ketoglutarate, while 3MP serves as a substrate for 3MST to produce H_2S. H_2S concentrations in the culture medium were measured using a H_2S-sensitive electrode (World Precision Instruments). The H_2S concentrations were calculated against the calibration curves of standard H_2S solutions. The amount of H_2S produced per microgram cell protein per minute was calculated as the activity of these H_2S-generating enzymes.

2.20. Immunofluorescence staining

Cells were fixed with 4% paraformaldehyde at 4 °C for 10 min. After washing and pre-blocking, the cells were incubated at 4 °C overnight with antibodies against Monoclonal anti-human Nrf2 followed by incubation with the FITC-conjugated secondary antibody (1:50; CST) for 1 h. DAPI was used for nuclear staining (10 μg/ml in PBS, Invitrogen). Images were then analyzed by laser confocal microscopy (Leica Sp5 Laser Scanning Confocal Microscope).

2.21. Patients and specimens

214 cases of GC cancer tissue specimens were recently obtained from patients undergoing surgical resection in Tongji Hospital affiliated to Tongji University (Shanghai, China). All patients were histologically confirmed and no radiotherapy or neoadjuvant chemotherapy had been administered before surgery. Informed consent was approved by the Ethics Committees of Tongji Hospital and all subjects gave written informed consent.

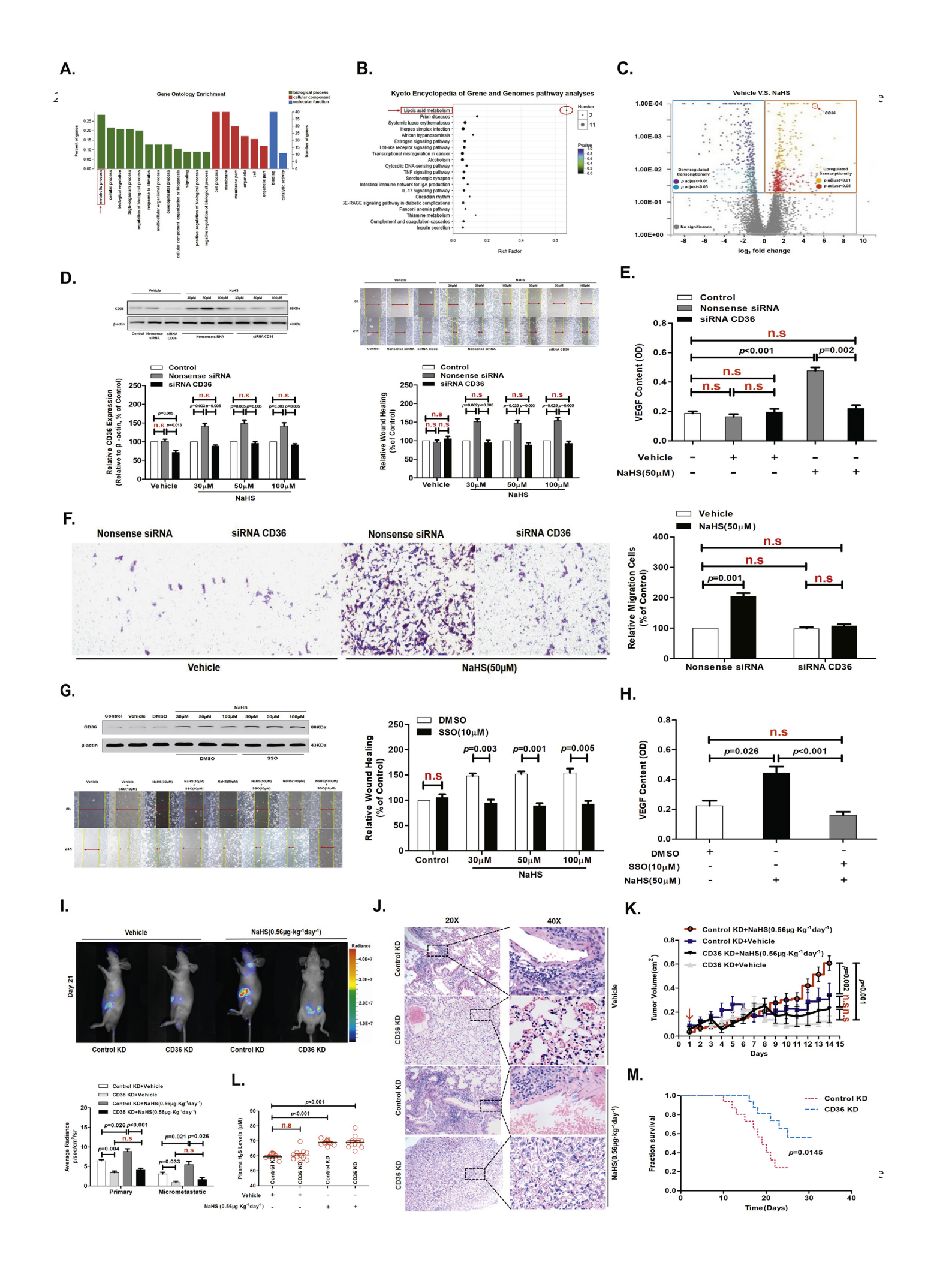
A.
Gene Ontology Enrichment
biological process
cellular component
molecular function
Percent of genes
Number of genes
metabolic process
cellular process
biological regulation
Sigle-organism process
regulation of biological process
response to stimulus
multicellular organismal process
developmental process
cellular component organization or biogenesis
signaling
positive regulation of biological process
negative regulation of biological process
cell process
membrane
membrane part
organelle
cell
organelle part
binding
catalytic activity
B.
Kyoto Encyclopedia of Grene and Genomes pathway analyses
Lipoic acid metabolism
Prion diseases
Systemic lupus erythematosus
Herpes simplex infection
African trypanosomiasis
Estrogen signaling pathway
Toll-like receptor signaling pathway
Transcriptional misregulation in cancer
Alcoholism
Cytosolic DNA-sensing pathway
TNF signaling pathway
Serotonergic synapse
Intestinal immune network for IgA production
IL-17 signaling pathway
Circadian rhythm
iE-RAGE signaling pathway in diabetic complications
Fanconi anemia pathway
Thiamine metabolism
Complement and coagulation cascades
Insulin secretion
Number
Pvalue
Rich Factor
C.
Vehicle V.S. NaHS
CD36
Downregulated transcriptionally
Upregulated transcriptionally
p adjust<0.01
p adjust<0.05
No significance
log2 fold change
D.
Vehicle
NaHS
30μM
50μM
100μM
CD36
β-actin
88KDa
43KDa
Control
Nonsense siRNA
siRNA CD36
Relative CD36 Expression (Relative to β-actin, % of Control)
Relative Wound Healing (% of Control)
Vehicle
NaHS
E.
Control
Nonsense siRNA
siRNA CD36
VEGF Content (OD)
n.s
p<0.001
p=0.002
Vehicle
NaHS(50μM)
F.
Nonsense siRNA
siRNA CD36
Vehicle
NaHS(50μM)
Relative Migration Cells (% of Control)
p=0.001
Nonsense siRNA
siRNA CD36
G.
Control
Vehicle
DMSO
SSO
DMSO
SSO(10μM)
Relative Wound Healing (% of Control)
p=0.003
p=0.001
p=0.005
H.
VEGF Content (OD)
p=0.026
p<0.001
DMSO
SSO(10μM)
NaHS(50μM)
I.
Vehicle
NaHS(0.56μg·kg-1day-1)
Day 21
Radiance
Control KD
CD36 KD
Control KD+Vehicle
CD36 KD+Vehicle
Control KD+NaHS(0.56μg·Kg-1day-1)
CD36 KD+NaHS(0.56μg·Kg-1day-1)
Average Radiance p/sec/cm2/sr
Primary
Micrometastatic
J.
20X
40X
Control KD
CD36 KD
Vehicle
NaHS(0.56μg·kg-1day-1)
K.
Control KD+NaHS(0.56μg·Kg-1day-1)
Control KD+Vehicle
CD36 KD+NaHS(0.56μg·Kg-1day-1)
CD36 KD+Vehicle
Tumor Volume(cm2)
Days
p<0.001
p=0.002
n.s
L.
Plasma H2S Levels (μM)
Vehicle
NaHS (0.56μg·Kg-1day-1)
M.
Control KD
CD36 KD
Fraction survival
p=0.0145
Time (Days)

performed using SPSS Statistics 19.0. Differences among three or more conditions were analyzed by one-way analysis of variance (ANOVA). Two-condition were analyzed with the Student's *t*-test. Significance was established at the $p < .05$ level.

3. Results

3.1. CD36 as a direct target molecule for H_2S-mediated acceleration of GC metastasis

We used RNA-Seq to identify potential differences in gene expression levels between treated with vehicle (normal saline, 0.9%) and 50 μM sodium hydrosulfide (NaHS; a donor molecule that rapidly releases H_2S) using AGS cells for 24 h (Fig. S1A). GO enrichment and KEGG pathway analyses revealed that the lipid metabolism pathway was one of the most differentially modulated pathways in AGS cells treated with NaHS (50 μM) for 24 h (Fig. 1A and B). By comparing the transcriptional profiles of AGS cells treated with NaHS (50 μM) for 24 h *versus* vehicle (Fig. S1B and 1C), we found that H_2S significantly up-regulated CD36 expression in GC cells at both the mRNA and protein levels (Fig. S1C and 1D), promoted GC-cell migration, invasion and increased vascular endothelial growth factor (VEGF) release (Fig. 1D-1F, Fig. S1D and S1E).

CD36 has been demonstrated to be involved in metastasis of GC indicating its pro-metastasis properties [18,30,31]. Therefore, in order to determine if CD36 expression is involved in the migration of GC cells in a CD36-dependent manner and whether it could be influenced by the effect of 10 μM sulfo-N-succinimidyl (SSO, CD36 inhibitor) or siRNA CD36 on cell migration, we selected 6 types of GC cell lines-AGS, HGC27, KATO III, NCI-N87, MGC803, SGC7901 cells, and human gastric epithelial cells-GES-1 cells. Among these GC cell lines, the migration of KATO III and NCI-N87 cells can be reduced by SSO (10 μM) or siRNA CD36, while AGS, HGC27, MGC803 and SGC7901 cells are not sensitive to SSO (10 μM) or siRNA CD36. We compared CD36 protein expression in these GC cell types (Fig. S1G). The CD36 protein expression level, is highest in KATO III and NCI-N87 cells, and lowest in AGS, HGC27, MGC803, and SGC7901 cells, indicating that the sensitivity of SSO (10 μM) or siRNA CD36 to the migration of GC cells is related to the level of cellular CD36 protein expression. This result also implies that the level of CD36 protein expression can be manipulated to inhibit KATO III and NCI-N87 cells or activate AGS and HGC27 cells by transfecting the siRNA CD36 or wild-type CD36 expression vectors. Therefore, we decided to use AGS and HGC27 cells to complete the rest of the experiments in this study.

In a separate series of experiments, to test whether H_2S promoted GC cell migration and VEGF release by targeted CD36, we examined cell migration and VEGF release in the presence or absence of SSO. We found that the promoting effect of H_2S was abolished after SSO (10 μM) treatment for 24 h (Fig. 1G and H). Next, we transfected AGS cells with siRNA specific to CD36 to inhibit receptor function. NaHS-treated cells containing CD36-specific siRNA showed a significant inhibition of H_2S-mediated cell migration, invasion and VEGF release compared with the cells transfected with nonsense siRNA *in vitro* (Fig. 1D-1F, Fig. S1D and S1E).

We next used an orthotopic xenotransplantation tumor model and a subcutaneous xenograft tumor model with the luciferase-labeled control KD and CD36 KD AGS cells (control KD and CD36 KD AGS-luc) in mice to assess the role of CD36 in H_2S-mediated metastasis *in vivo* (Fig. S1F). On the 3 weeks after upon orthotopic injection of control KD and CD36 KD AGS-luc, we found a significant increase in the bioluminescent radiation volume in the tumor-bearing, NaHS (0.56 $\mu g \cdot kg^{-1} \cdot day^{-1}$)-treated control KD AGS-luc cells mice compared with that of CD36 KD AGS-luc cells mice, indicating that H_2S promoted metastasis (Fig. 1I). When the experiment was terminated, major organs in each group were dissected and examined for metastases. Metastasis to the lungs was significantly increased in control KD AGS-luc cells mice that received NaHS (0.56 $\mu g \cdot kg^{-1}$ day^{-1}) treatment for 3 weeks in orthotopic xenotransplantation tumor model (Fig. 1J). Additionally, tumor weight was markedly increased after 3 weeks of NaHS (0.56 $\mu g \cdot kg^{-1}$ day^{-1}) treatment compared with CD36 KD AGS-luc cells mice in subcutaneous xenograft tumor model (Fig. 1K). In addition, GC progression in these mice was analyzed weekly by live-animal bioluminescence, which revealed that there was a consistently reduced tumor burden in mice bearing CD36 KD AGS-luc cells with NaHS (0.56 $\mu g \cdot kg^{-1}$ day^{-1}) treatment compared with that of control KD AGS-luc cells mice (Fig. 1I). Mice transplanted with CD36 KD AGS-luc cells had a significantly increased survival time compared to those bearing control KD AGS-luc cells in orthotopic xenotransplantation tumor model (Fig. 1M). Therefore, targeting CD36 *in vivo* blocked H_2S-promoted GC metastasis and improved animal survival. Finally, we detected the level of H_2S in the plasma of mice; NaHS (0.56 $\mu g \cdot kg^{-1}$ day^{-1})-treated mice every other day showed significantly higher H_2S levels (average 71.26 μM H_2S) than vehicle-treated mice (average 59.36 μM H_2S) in orthotopic xenotransplantation tumor model (Fig. 1L). These results suggested that the CD36 as a direct target molecule for H_2S-mediated acceleration of GC metastasis.

In our previous studies, we examined the effects of H_2S in human umbilical vein endothelial cells (HUVEC) and found that H_2S could promote the migration of HUVEC [6]. We also tested the effect of H_2S on GES-1 cells. We found that H_2S could not promote GES-1 cell migration and the release of VEGF was reduced with a 24-h NaHS (50 μM) treatment in GES-1 cells (Fig. S2A and S2B). In addition, the protein expression level of the VEGF receptor-2 (VEGFR-2) was low in GC cells and following treatment with various concentrations of NaHS for 24 h, we concluded that VEGFR2 was not regulated by H_2S. These data implicated CD36 as a direct target molecule for H_2S-accelerated GC metastasis.

3.2. CD36 overexpression induced reprogramming of lipid metabolism and promoted GC metastasis

The panel of GC cells on which we conducted metabolic analysis showed wide variations in the metabolic phenotype of the individual GC cell lines. Interestingly, the subgroup of cell lines with $CD36^{low}$ showed a similar metabolic index indicative of lower reliance on mitochondrial ATP production (Fig. 2A, H and I). To understand the role of CD36 in GC cell metabolism, we examined the FAO and ECAR of GC cells stably expressing wild-type (wt) CD36 as metabolism assayed by Seahorse analysis. We found that CD36(wt) overexpression significantly promoted LC-FA uptake measured using a chemiluminescence assay (Fig. 2B) and reinforced cellular FAO (Fig. 2C). CD36(wt) overexpression also improved ATP production as metabolism assayed by

Fig. 1. CD36 as a direct target molecule for H_2S-mediated acceleration of GC metastasis. (A) GO Enrichment. (B) KEGG pathway analyses. (C) 2D-plots of total genes in vehicle (Normal Saline, 0.9%)-and NaHS (50 μM)-treated cells measured by RNA-Seq. Up- and down-regulated genes with NaHS treatment are highlighted. (D) Western blots showing CD36 protein levels in AGS cells. H_2S promoted cell migration in the nonsense siRNA groups and this effect was inhibited in cells with CD36-specific siRNA knockdown (n = 10, student's *t*-test). (E) H_2S induced AGS cells to release VEGF in nonsense siRNA groups, but this effect was inhibited in cells with CD36-specific siRNA knockdown (n = 3, student's t-test). (F) Transwell assays showing the promoting effects of H_2S on cell invasion in serum-free, stimulated GC cells (n = 10, student's t-test). (G) Western blots showing CD36 protein levels in AGS cells, with H_2S promoting cell migration in the vehicle groups. This effect was abolished by the CD36 receptor inhibitor (SSO) treatment (n = 10, student's t-test). (H) H_2S induced AGS cells to release VEGF in the vehicle groups, but this effect was abolished by SSO treatment (n = 3, student's t-test). (I) Representative bioluminescence imaging of metastatic nodules in mice with orthotopic xenotransplantation tumor model (n = 3 groups and 4 mice in each group, student's *t*-test). (J) Effect of H_2S on lung metastasis of GC cells in mice with orthotopic xenotransplantation. (K) The curve of tumor growth after a 15-day treatment with NaHS in mice with subcutaneous xenograft tumor model (n = 3 groups and 4 mice in each group, student's *t*-test). (L) The level of H_2S in the plasma of orthotropic xenotransplanted mice (student's t-test). (M) The survival of mice injected with either control KD or CD36 KD AGS-luc cells in mice with orthotopic xenotransplantation tumor model (student's t-test). n.s, no significant differences. Each bar represents the mean ± standard deviation (S.D.).

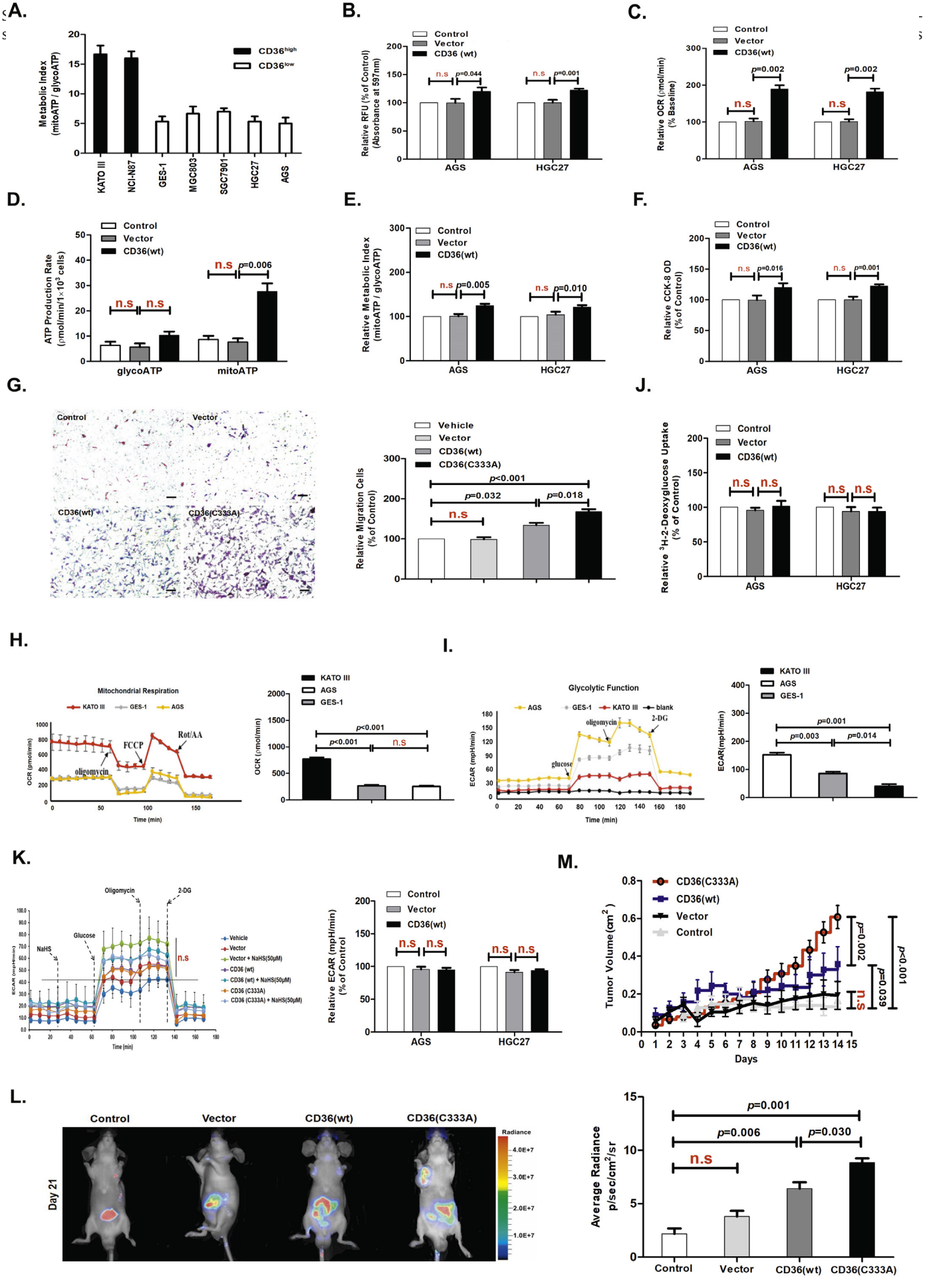
A.
Metabolic Index (mitoATP / glycoATP)
CD36high
CD36low
KATO III
NCI-N87
GES-1
MGC803
SGC7901
HGC27
AGS
B.
Control
Vector
CD36 (wt)
Relative RFU (% of Control) (Absorbance at 597nm)
n.s p=0.044
n.s p=0.001
AGS
HGC27
C.
Control
Vector
CD36(wt)
Relative OCR (pmol/min) (% Baseline)
p=0.002
p=0.002
n.s
n.s
AGS
HGC27
D.
Control
Vector
CD36(wt)
ATP Production Rate (pmol/min/1×10³ cells)
n.s
n.s
n.s p=0.006
glycoATP
mitoATP
E.
Control
Vector
CD36(wt)
Relative Metabolic Index (mitoATP / glycoATP)
n.s p=0.005
n.s p=0.010
AGS
HGC27
F.
Control
Vector
CD36(wt)
Relative CCK-8 OD (%of Control)
n.s p=0.016
n.s p=0.001
AGS
HGC27
G.
Control
Vector
CD36(wt)
CD36(C333A)
Vehicle
Vector
CD36(wt)
CD36(C333A)
Relative Migration Cells (% of Control)
p<0.001
p=0.032
p=0.018
n.s
J.
Control
Vector
CD36(wt)
Relative ³H-2-Deoxyglucose Uptake (% of Control)
n.s n.s
n.s n.s
AGS
HGC27
H.
Mitochondrial Respiration
KATO III
GES-1
AGS
OCR (pmol/min)
FCCP
Rot/AA
oligomycin
Time (min)
KATO III
AGS
GES-1
OCR (pmol/min)
p<0.001
p<0.001
n.s
I.
Glycolytic Function
AGS
GES-1
KATO III
blank
ECAR (mpH/min)
oligomycin
2-DG
glucose
Time (min)
KATO III
AGS
GES-1
ECAR(mpH/min)
p=0.001
p=0.003
p=0.014
K.
Oligomycin
2-DG
Glucose
NaHS
n.s
ECAR (mpH/min)
Time (min)
Vehicle
Vector
Vector + NaHS(50μM)
CD36 (wt)
CD36 (wt) + NaHS(50μM)
CD36 (C333A)
CD36 (C333A) + NaHS(50μM)
Control
Vector
CD36(wt)
Relative ECAR (mpH/min) (% of Control)
n.s n.s
n.s n.s
AGS
HGC27
M.
CD36(C333A)
CD36(wt)
Vector
Control
Tumor Volume (cm²)
p=0.002
n.s
p=0.039
p<0.001
Days
L.
Control
Vector
CD36(wt)
CD36(C333A)
Day 21
Radiance
4.0E+7
3.0E+7
2.0E+7
1.0E+7
Average Radiance p/sec/cm²/sr
p=0.001
p=0.006
p=0.030
n.s
Control
Vector
CD36(wt)
CD36(C333A)

(Fig. 3C and 2G). Moreover, we found that CD36(wt) overexpression had no significant effect on glucose uptake and glycolysis function in GC cells, as assessed by a 2-deoxyglucose uptake assay and metabolism assay, respectively (Fig. 2J and K). These data suggested that CD36 overexpression in GC cells with lower CD36 expression, induced reprogramming of lipid metabolism *in vitro*.

To determine if CD36-mediated elevation of metastasis occurs *in vivo*, we engrafted mice with AGS-luc cells transfected with empty-vector or CD36(wt). We found that CD36(wt)-containing AGS-luc cells significantly promoted cellular metastasis after 3 weeks in orthotopic xenotransplantation tumor model (Fig. 2L). Additionally, tumor weight after 3 weeks was markedly increased in mice transplanted with CD36 (wt)-containing AGS-luc cells compared with empty-vector AGS-luc cells in subcutaneous xenograft tumor model (Fig. 2M). Taken together, these data implicated CD36 overexpression in GC cells with lower CD36 expression, promoted GC metastasis *in vivo*.

3.3. A disulfide bond between Cys333-Cys272 of CD36 can be cleaved by H_2S to enhance bioenergetic processes

Electrospray ionization (ESI) collision-induced dissociation (CID)-MS-MS analysis of CD36 revealed the presence of a disulfide bond within its structure, located between two Cys at amino acid 333 and 272. Fig. 3A shows a precursor ion molecule of $[M + 3H]^{3+}$ m/z 525.22 that yielded a series of CID fragments that matched the CID-induced y-ions of two trypsin-digested peptide ions (designated as the α and the β peptide), namely QVLQFFSSDIC^{272} ($y1^{\alpha}$-$y4^{\alpha}$) and C^{333}K ($y1^{\beta}$-$y4^{\beta}$). This illustrated that these two peptides are joined together by a covalent bond. An additional series of CID induced y-ions were also identified that contained the Cys272 residue within the polypeptide chains, including the α peptide bound with an additional sulfur atom ($[M + H]^+$ m/z 521.31), the α peptide bound with an additional Cys residue ($[M + H]^+$ m/z 175.12), and the α peptide bound with a Cys residue where an isoleucine residue (adjacent to Cys333 on the N-terminal side) was bound ($[M + H]^+$ m/z 147.11). These data confirmed that the covalent bond was localized between the two Cys residues (Cys333 and Cys272). Interestingly, treatment of these peptides with 50 μM NaHS for 24 h induced the breaking of the disulfide bond between Cys333 and Cys272 (Fig. 3B). To test the role of this disulfide bond within CD36 in AGS cell migration, we examined the migration of AGS cells that stably expressed a mutant form of CD36. We found that stable expression of CD36(C333A) in AGS cells significantly promoted migration compared with cells expressing CD36(wt), CD36(C311A), or CD36(C322A) (Fig. 3C).

H_2S in solution is composed of a mixture of H_2S gas and the HS^- anion in a dynamic equilibrium. This equilibrium is pH sensitive, with acidification reducing the concentration of the HS^- anion and increasing that of the H_2S gas. In our previous studies, NaHS, GSH, Cys, Cys-Gly, and homocysteine were each allowed to react with a model chemical (a synthesized hexapeptide containing a disulfide bond) at concentrations with equal reducing potency. The hexapeptide was applied at equal concentrations to each reaction and thus the peaks of the hexapeptide also served as an internal standard for quantification of the ion peaks in the MS analysis. The products yielded from cleaving the disulfide bond of the hexapeptide were quantified as the ratio of the product peaks to the hexapeptide peaks. The result illustrated that NaHS was the most efficient in reducing the disulfide bond [6].

To further examine the capabilities of H_2S, we re-examined its disulfide bond-breaking effects under a range of pH values. We found that cleavage of the disulfide bond occurred at pH values ≥7.0 with 50 μM NaHS for 24 h, while cleavage was completely blocked at pH values ≤5.5 (Fig. 3D-3F). This finding suggested that the ability of H_2S to break disulfide bonds is largely due to the HS^- anion and not H_2S gas. This finding also indicated that the breaking of the disulfide bond is a reversible chemical process akin to that described for several redox-sensitive proteins.

Based on our data, the regulation of FAO has an important role in GC cells after NaHS treatment. Accordingly, NaHS (50 μM) treatment of AGS cells for 24 h significantly heightened the cellular levels of ROS measured by DCFH-DA staining. DCFH-DA undergoes hydrolysis and then ROS-mediated oxidation to a fluorescent state, providing a measure of ROS levels in cells. This increased ROS generation can also be qualitatively appreciated in cells with NaHS (50 μM) treatment using fluorescence intensity assay detected by a fluorescence microscope (Fig. 6G). NaHS (50 μM) treatment for 24 h also significantly promoted FAO and ATP production by metabolism assay in AGS cells (Fig. 3H and I). The CD36(C333A) mutant caused a significant increase in the levels of ROS, FAO, and ATP production (Fig. 3G-3I). However, NaHS (50 μM) treatment for 24 h was not able to raise the levels of FAO and ATP production in AGS cells stably expressing CD36(C333A). Nevertheless, in the control cells expressing CD36(wt), NaHS (50 μM) treatment for 24 h was still able to improve the levels of FAO and ATP production (Fig. 3H and I). Therefore, these data suggested that a disulfide bond between Cys333-Cys272 of CD36 can be cleaved by H_2S to enhance bioenergetic processes.

3.4. H_2S activated the second LC-FA binding conformation of CD36

Quantum chemical calculations and ESI-MS were performed to investigate how the HS^- anion breaks the disulfide (S—S) bond. Our previous results revealed a two-part reaction:

$$\text{Reaction 1}: HS^- + C_3H_6NO_2{-}S{-}S{-}C_3H_6NO_2 \rightarrow C_3H_6NO_2{-}S^- + HS{-}S{-}C_3H_6NO_2$$

$$\text{Reaction 2}: HS^- + HS{-}S{-}C3H_6NO_2 \rightarrow C_3H_6NO_2{-}S^- + HS{-}SH$$

Each of the reactions was initiated by the nucleophilic attack of the HS^- anion on the disulfide bond. HS^- attacked the disulfide bond *via* an interaction with its frontier molecular orbitals [6].

The CD36 ectodomain adopts an architecture similar to Lysosomal Integral Membrane Protein (LIMP)-2 (Fig. 4A); however, unlike LIMP-2, the cavity of CD36 contains two election-density features that resemble the extended hydrocarbon chain of LC-FAs (Fig. S3A) [32]. The entrance for the LC-FA translocation pathway has previously been proposed to lie close to lysine (Lys) 164 [33]. Indeed, the central cavity of CD36 has an opening close to this residue (entrance 1) that is a likely entry point for the membrane-distal LC-FAs and is the entrance whose

Fig. 2. CD36 overexpression induced reprogramming of lipid metabolism. (A) Evaluation of the metabolic index (mitochondrial ATP: glycolytic ATP production rate) of a panel of human GC cell lines. (B) Chemiluminescence assay detecting the LC-FA uptake capacity of AGS and HGC27 cells stably overexpressing CD36(wt) (n = 3, student's *t*-test). (C) Seahorse assay evaluating the level of FAO in AGS and HGC27 cells stably overexpressing CD36(wt) (n = 3, student's *t*-test). (D) Real-time bioenergetics assay (Seahorse assay) showing the ATP production rate in AGS and HGC27 cells stably overexpressing CD36(wt) (n = 3, student's *t*-test). (E) Seahorse assay evaluating the metabolic index of AGS cells and HGC27 cells stably expressing CD36(wt) (n = 3, student's t-test). (F) CCK-8 assay measuring cell viability in AGS and HGC27 cells stably overexpressing CD36(wt) (n = 3, student's *t*-test). (G) Transwell assay showing the promoting effects of overexpressing CD36 and Cys333 mutation on cell invasion in serum-free, stimulated GC cells (n = 6, student's *t*-test). (H) Seahorse assay evaluating the mitochondrial respiration in KATO III, GES-1, and AGS cells (n = 3, student's t-test). (I) Seahorse assay evaluating the glycolysis function in KATO III, GES-1, and AGS cells (n = 3, student's *t*-test). (J) 2-deoxyglucose uptake assay in AGS and HGC27 cells stably overexpressing CD36(wt) (n = 3, student's *t*-test). (K) Seahorse assay evaluating glycolysis function in AGS and HGC27 cells (n = 3, student's *t*-test). (L) Bioluminescence imaging analysis of metastatic nodules in mice with orthotopic xenotransplantation tumor model (n = 3 groups and 4 mice in each group, student's *t*-test). (M) The curve of tumor growth after a 15-day treatment with NaHS in mice with subcutaneous xenograft tumor model (n = 3 groups and 4 mice in each group, student's t-test). n.s, no significant differences. Each bar represents the mean ± standard deviation (S.D.).

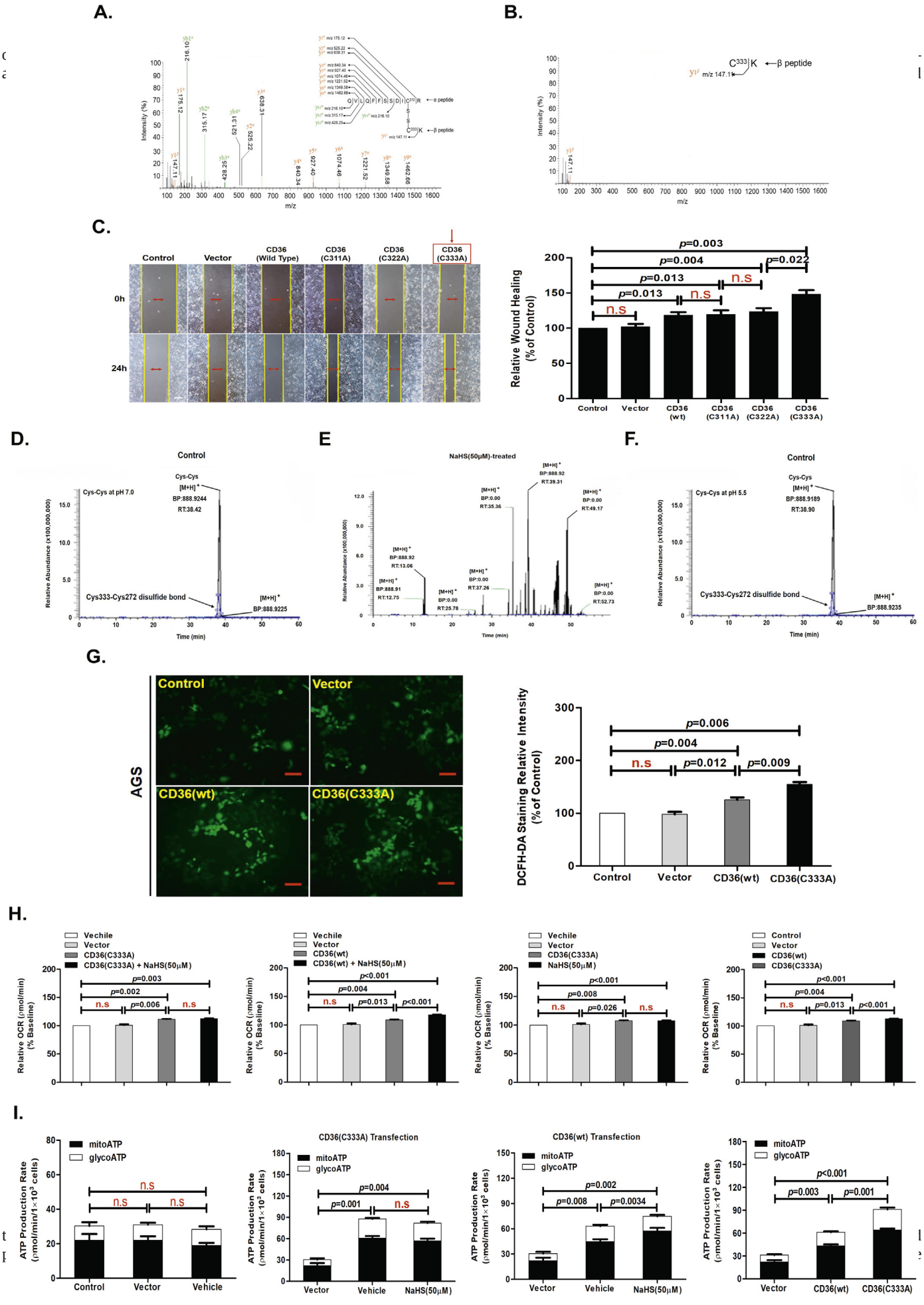
A.
B.
C.
Control
Vector
CD36 (Wild Type)
CD36 (C311A)
CD36 (C322A)
CD36 (C333A)
0h
24h
Relative Wound Healing (% of Control)
p=0.003
p=0.004
p=0.022
p=0.013
n.s
p=0.013
n.s
n.s
CD36 (wt)
D.
E.
F.
Control
NaHS(50μM)-treated
Cys-Cys at pH 7.0
Cys-Cys at pH 5.5
Cys333-Cys272 disulfide bond
Relative Abundance
Time (min)
G.
AGS
CD36(wt)
CD36(C333A)
DCFH-DA Staining Relative Intensity (% of Control)
p=0.006
p=0.004
n.s
p=0.012
p=0.009
H.
Vechile
CD36(C333A)
CD36(C333A) + NaHS(50μM)
CD36(wt)
CD36(wt) + NaHS(50μM)
NaHS(50μM)
Relative OCR (pmol/min) (% Baseline)
I.
mitoATP
glycoATP
ATP Production Rate (pmol/min/1×10³ cells)
CD36(C333A) Transfection
CD36(wt) Transfection
Vehicle
NaHS(50μM)

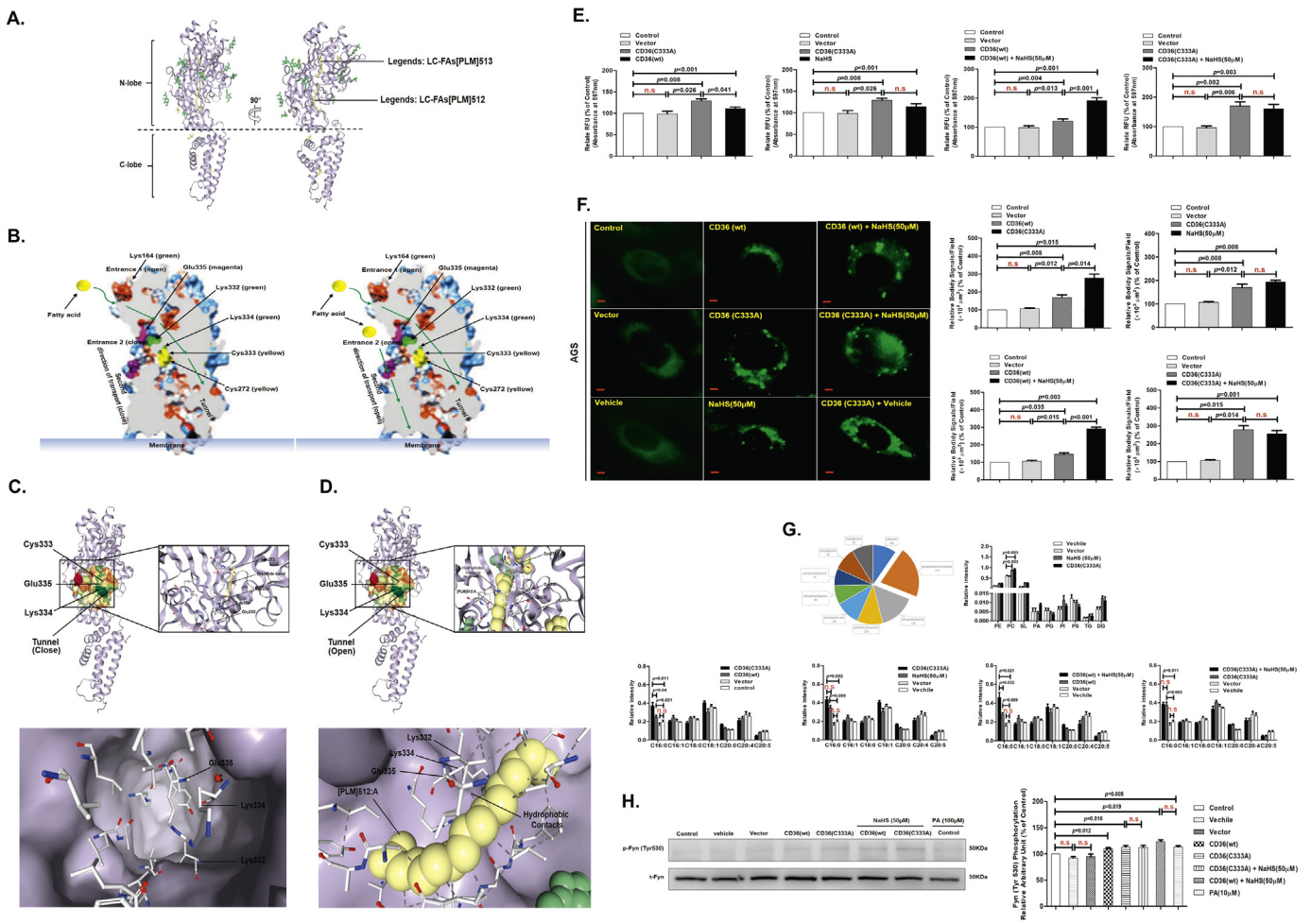

Fig. 4. H_2S activated the second LC-FA binding conformation of CD36. (A) The structure of CD36 is shown in purple. The nine N-linked glycosylation sites and associated sugars are in green, and the two palmitic acids are shown as yellow sticks. (B) A section through a surface representation of CD36 showing the control core cavity occupied by LC-FAs at entrance 1 (green arrows). The insets show putative entry points to this central cavity at entrance 2. (C) When the Cys333-Cys272 disulfide bond is present in CD36, the Lys334 and Glu335 salt bridge is disrupted, limiting LC-FA interaction with the carboxyl groups of Lys334 within CD36. (D) Secondary-structure prediction using the I-TASSER platform suggests that Lys334 and Lys332 are localized in a turn between helical and sheet structures on the edge of the hydrophobic pocket within CD36. There is a conserved salt bridge between Lys334 and Glu335. Lys332 increases the hydrophobicity of the binding pocket and helps position the LC-FA interaction with the carboxyl groups of Lys334 within CD36. In the absence of the Cys333-Cys272 disulfide bond, Lys334 would be exposed to the solvent and could dock LC-FAs into the hydrophobic pocket. (E) Chemiluminescence assay showing the effects of Cys333 mutation on the LC-FA uptake capacity of CD36 (n = 3, student's *t*-test). (F) Bodipy Staining analysis showing the effects of Cys333 mutation on the LC-FA uptake capacity of CD36 (n = 3, student's t-test). (G) Metabolome study of the effects of Cys333 mutation on the LC-FA uptake capacity of CD36 (n = 3, student's t-test). (H) Western blot assays showing the effects of Cys333 mutation on Fyn phosphorylation of CD36 (n = 4, student's t-test). n.s, no significant differences. Each bar represents the mean ± standard deviation (S.D.).

SSO target residue Lys164, as well as residue Lys334, which is a second binding site and SSO target [33]. The residue Glu335 is positioned at the site of LC-FA entry into the tunnel. Lys334 may be important for correctly positioning the LC-FA within the hydrophobic binding pocket; this lysine may permit the LC-FA to slide into the tunnel *via* a conserved salt bridge between Lys334 and Glu335 and then induce a conformational change in the protein to initiate the signaling pathway.

We found that when the Cys333-Cys272 disulfide bond was present in CD36, its second LC-FA binding pocket was capped closed. The Cys333-Cys272 disulfide bond stabilized a turn in the CD36 protein between helical and sheet structures at N-terminal region, such that the extracellular region of the protein formed a "lid" at the entrance to the second LC-FA binding pocket (Fig. 4C). This "lid" blocked the movement of the LC-FA from the extracellular region of the CD36 receptor into the binding pocket. In this configuration, Lys334 was not exposed to the solvent and could not dock the LC-FA into the hydrophobic pocket, thereby preventing the release of the LC-FA into the cytoplasm. Thus, the activation of the second LC-FA binding conformation of CD36 requires the Cys333-Cys272 disulfide bond to be broken. When the Cys333-Cys272 disulfide bond was absent, the structures of Lys332 and Lys334 were similar to the structures of Lys164 and Lys166 (Fig. S3B); Lys334 was exposed to the solvent, it could dock the LC-FA into the hydrophobic pocket, and possibly permit it to slide into the tunnel by a conserved salt bridge between Lys334 and Glu335. Lys332 increased the hydrophobicity of the binding pocket and helped position the LC-FA to

Fig. 3. CD36 molecular structure contained a disulfide bond between Cys333-Cys272 that can be cleaved by H_2S to heighten bioenergetic processes. (A) ESI-CID-MS-MS spectra of CD36. (B) CID spectra of $[M + 3H]^{3+}$ 147.1100 from a TriPort digest of CD36 in the presence of NaHS, showing the β peptide containing Cys333. (C) Wound-healing assay showing the effects of Cys333, Cys313, and Cys322 mutations on migration capacity in AGS cells (n = 10, student's *t*-test). (D, E, and F) ESI-MS spectra showing cleavage of the disulfide bond in the CD36 molecular model chemical of Cys-Cys, in the absence or presence of NaHS or at pH values of 5.5. (G) DCFH-DA staining chemiluminescence assay showing the effects of Cys333 mutation on the level of ROS production in AGS cells (n = 3, student's *t*-test). (H and I) Seahorse assay examining the effect of Cys333 mutation on cellular metabolism. (H) FAO (n = 3, student's t-test). (I) ATP production (n = 3, student's t-test). n.s, no significant differences. Each bar represents the mean ± standard deviation (S.D.).

interact with Lys334 (Fig. 4D). This series of events finally permitted the LC-FA access to the cytoplasm from the extracellular milieu.

To test the role of the Cys333-Cys272 disulfide bond within CD36 in AGS cells, we examined LC-FA uptake in AGS cells stably expressing the mutant CD36. We were surprised to find that CD36(C333A) expression significantly increased the capacity of AGS cells to take in LC-FAs (measured by a chemiluminescence assay and bodipy (boron-dipyrromethene) staining) and the enhancing effect of H_2S disappeared entirely (Fig. 4E and F). MRM analysis revealed that palmitic acid (PA) was mostly a mixture of the LC-FAs present in AGS cells expressing CD36(C333A) (Fig. 4G). Western blot assays showed that the phosphorylation level of Fyn, a key non-receptor tyrosine kinase at the initial of the metastasis, was increased in CD36(C333A)-expressing AGS cells (Fig. 4H and Fig. S3C). Taken together, these data illustrated that the Cys333-Cys272 disulfide bond disrupted the integrity of the second LC-FA binding conformation of CD36, blocking the precise positioning required for LC-FA binding in the second entrance through CD36 to the cell cytoplasm.

3.5. Expression of CD36(C333A) promoted metastasis of GC cells and prevented the enhancing effect of H_2S

We measured MMP in AGS cells stably expressing CD36(C333A) using a TMRM probe assay *in vitro*. We found that CD36(C333A)-expressing AGS cells had significantly increased cellular MMP. In addition, NaHS (50 μM) treatment for 24 h revealed that the enhancing effect of H_2S completely disappeared in AGS cells expressing CD36 (C333A) (Fig. 5A). Moreover, cell migration and VEGF release were significantly increased in AGS cells stably expressing the mutant CD36 (C333A). Although H_2S had no effect, PA (10 ng/mL) still showed a promoting effect on cell migration (Fig. 5B and C, Fig. S3D and S3E). Subsequent CCK-8 assays and Transwell assay also confirmed these results (Fig. 5D and E).

In vivo, transplant of CD36(C333A)-expressing AGS-luc cells significantly promoted cellular metastasis in mice compared with the transplant of AGS-luc cells expressing empty-vector and CD36(wt) (Fig. 2L). Similar to the *in vitro* results, NaHS treatment (0.56 $\mu g \cdot kg^{-1} \cdot day^{-1}$ for 3 weeks) of mice injected with CD36(C333A)-expressing AGS-luc cells did not produce any metastasis-enhancing effect of H_2S in orthotopic xenotransplantation tumor model (Fig. 5F). NaHS treatment (0.56 $\mu g \cdot kg^{-1}$ day^{-1} for 3 weeks) of mice injected with CD36 (C333A)-expressing AGS-luc cells did not produce any tumor volume-enhancing effect of H_2S in subcutaneous xenograft tumor model (Fig. 5G). We also detected the level of H_2S in the plasma of mice; NaHS (0.56 $\mu g \cdot kg^{-1}$ day^{-1})-treated mice every other day showed significantly higher H_2S levels (average 72.16 μM H_2S) than vehicle-treated mice (average 56.18 μM H_2S) in orthotopic xenotransplantation

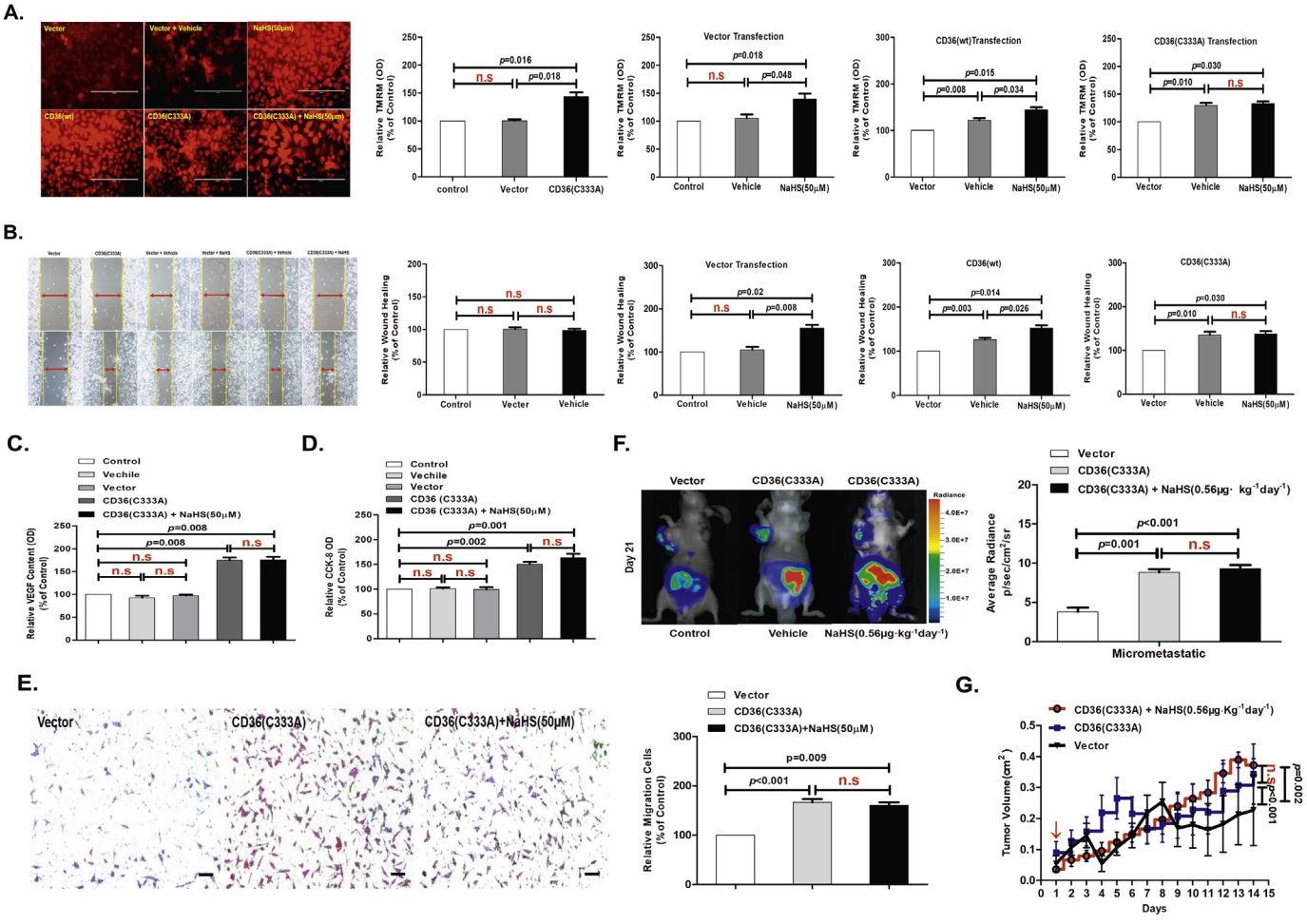

Fig. 5. Expression of CD36(C333A) promoted metastasis of GC cells and endogenous H_2S was required for CD36-induced antiangiogenic drug resistance. (A) TMRM analysis showing the effects of Cys333 mutation on mitochondrial membrane potential in AGS cells (n = 6, student's t-test). (B) Wound-healing assay showing the effects of Cys333 mutation on the migration of AGS cells (n = 10, student's t-test). (C) ELISA showing the effects of Cys333 mutation on VEGF release in AGS cells (n = 3, student's t-test). (D) CCK-8 assay showing the effects of Cys333 mutation on cell viability in AGS cells (n = 3, student's t-test). (E) Transwell assays showing the promoting effects of H_2S on cell invasion in serum-free, stimulated GC cells (n = 3, student's t-test). (F) Bioluminescence imaging analysis of metastatic nodules in mice with orthotopic xenotransplantation tumor model (n = 3 groups and 4 mice in each group, student's t-test). (G) The curve of tumor growth after a 15-day treatment with NaHS in mice with subcutaneous xenograft tumor model (n = 3 groups and 4 mice in each group, student's t-test). n.s, no significant differences. Each bar represents the mean ± standard deviation (S.D.).

tumor model (Fig. S3F). Taken together, these data not only indicated that the Cys333-Cys272 disulfide bond served as an intrinsic inhibitory motif, but they also implicated the disulfide bond as a specific molecular switch to activate the second LC-FA binding conformation in CD36, which is required to mediate H_2S-induced GC cell metastasis.

3.6. Endogenous H_2S was necessary for CD36-induced, antiangiogenic drug resistance

Antiangiogenic drug (AAD) resistance is a frequent problem in cancer patients [34–36]. AAD induces hypoxia, increases lipolysis, and accelerates cancer cell metastasis [37–39]. To explore the role of H_2S in hypoxia-induced cancer cell migration, we implemented a wound-healing assay to show that moderate hypoxia for 24 h (depriving the culture medium from 20% dissolving oxygen) caused a significant enhancement of migration of colon cancer cells and AGS cells (Fig. 6A) [40]. Activity of the endogenous H_2S-generating enzyme, CSE, as well as the expression of CD36, was increased in AGS cells cultured under moderate hypoxic conditions as compared with cells cultured under normoxic conditions (Fig. 6B and S3G). In contrast, activity of the endogenous H_2S-generating enzyme 3MST was decreased in AGS cells cultured under moderate hypoxic conditions as compared with cells cultured under normoxic conditions (Fig. 6C). Activity of the endogenous H_2S-generating enzyme CBS was not significantly changed in the AGS cells cultured under moderate hypoxic conditions as compared with normoxic conditions (Fig. 6D). Moreover, siRNA-mediated knockdown of CSE attenuated the hypoxia (or LC-FA)-induced increase in the migration of AGS cells for 24 h, and NaHS (50 μM) treatment could rescue that siRNA-mediated knockdown of CSE attenuated the hypoxia (or LC-FA)-induced increase in the migration of AGS cells for 24 h (Fig. 6E and F, Fig. S3G). Quantification of ROS measured by DCFH-DA staining showed that total intracellular ROS levels were significantly increased in fast-migrating AGS cells compared with slow-migrating AGS cells for 24 h (Fig. 6G). This observation illustrated that a transient, oxidizing, intracellular environment may occur during antiangiogenic-drug resistance [37]. Taken together, these results suggested that CD36 mediated endogenous H_2S-promoted migration in antiangiogenic-drug resistance.

In our previous studies, we found that CSE and VEGFR2 were colocalized at the membrane of HUVEC [6]. To further determine the clinical relevance of our finding that H_2S promotes cancer cell metastasis, we performed IHC analyses to examine the levels of CSE and CD36 in serial sections of 214 case human GC specimens. Staining quantification showed CSE levels was positively correlated with CD36 expression levels (Fig. 6H). No case in the normal control showed significant CSE and CD36 signals (Fig. S2D). As illustrated in supplementary table S1, the expression rate of CSE was higher in female than in male, and was increased as the TNM stage increased. Surprisingly, the expression

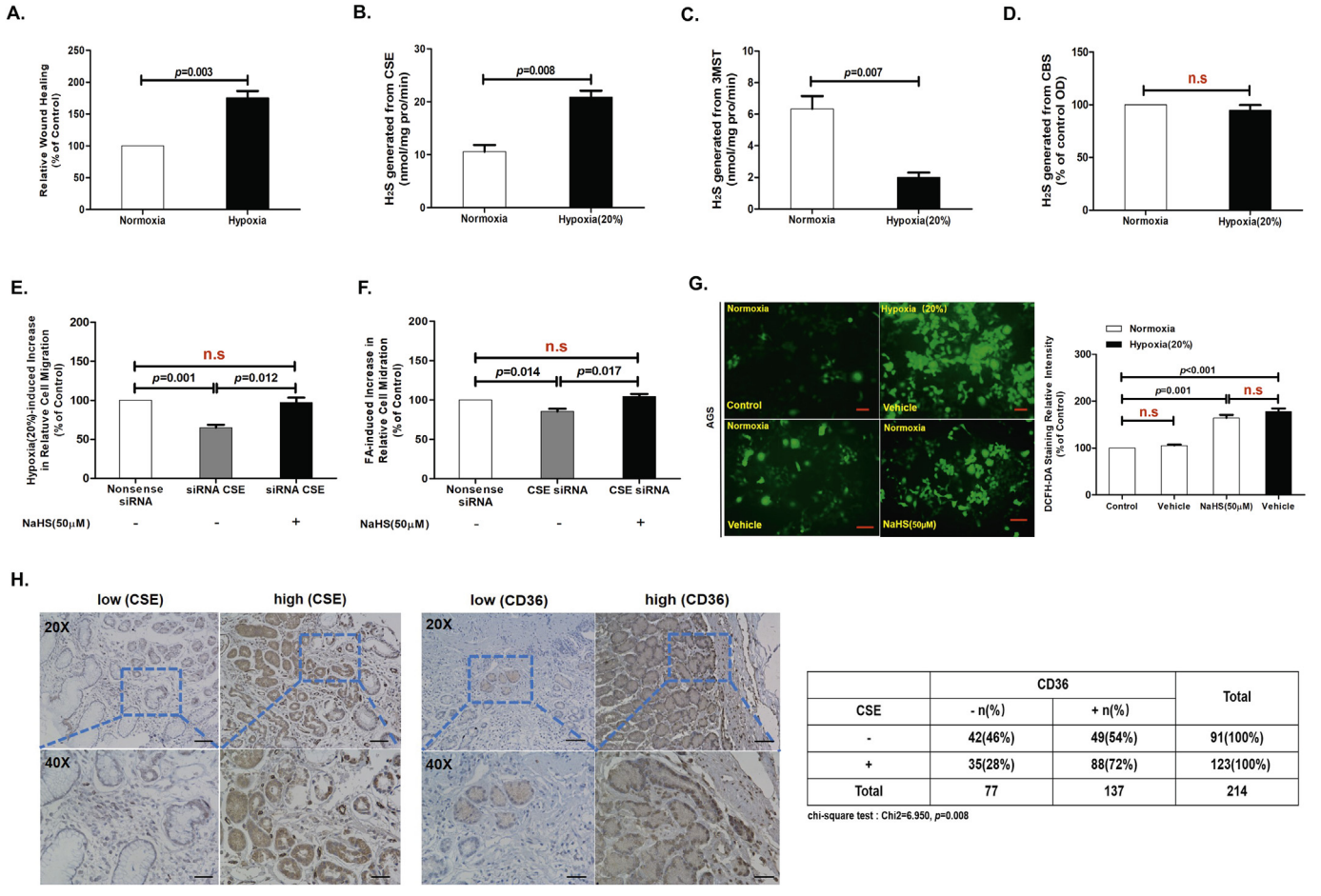

CSE	CD36 - n(%)	CD36 + n(%)	Total
-	42(46%)	49(54%)	91(100%)
+	35(28%)	88(72%)	123(100%)
Total	77	137	214

chi-square test : Chi2=6.950, p=0.008

Fig. 6. Endogenous H_2S was necessary for CD36-induced, antiangiogenic drug resistance. (A) Moderate hypoxia could significantly promote the migration of AGS cells (n = 3, student's t-test). (B) The activity of the endogenous, H_2S-producing enzyme CSE was elevated by moderate hypoxia (n = 3, student's t-test). (C) The activity of the endogenous, H_2S-producing enzyme 3MST was elevated by moderate hypoxia (n = 3, student's t-test). (D) The activity of the endogenous, H_2S-producing enzyme CBS was elevated by moderate hypoxia (n = 3, student's t-test). (E, F) Moderate hypoxia could significantly promote the migration of AGS cells and this migration-promoting effect was significantly decreased by CSE-specific siRNA. siRNA-mediated knockdown of CSE attenuated the LC-FA-induced increase in the migration of AGS cells (n = 6, student's t-test). (G) DCFH-DA staining chemiluminescence assay showing the effects of hypoxia on ROS production in AGS cells (n = 3, student's t-test). (H) Immunohistochemical staining with anti-CSE and anti-CD36 antibodies was performed on 214 human stomach tumor specimens. Scale bar: 20 μm (left and right panels). Relation between categorized variables was examined by Chi-square test. n.s, no significant differences. Each bar represents the mean ± standard deviation (S.D.).

levels of CSE was related to the history of Helicobacter pylori infection. However, the proportions were similar between different age, histology, and tumor size.

3.7. H_2S up-regulated protein expression levels of CD36 by induced Nrf2 nuclear translocation

Initial studies conducted a biological role for H_2S in mammals in which H_2S was shown to promote the relaxation of vascular smooth muscles [41]. This pioneering study reveal an important physiological role for H_2S in the cardiovascular system. The present study showed that Nrf2 promotes tumor maintenance by modulating mRNA translation in pancreatic cancer [42], and H_2S induces Nrf2-target genes by inactivating the Keap-1 ubiquitin ligase substrate adaptor through formation of a disulfide bond between Cys226 and Cys613 [43].

To further confirmed that H_2S induces Nrf2-target gene CD36 expression in GC cells, we detected the protein expression levels of Nrf2 in AGS cells with NaHS treatment on different concentrations for 24 h by western blot assay. We found that the protein expression levels of Nrf2 was not a concentration-dependent progressive augmentation in the whole cell extracts from AGS cells treated with NaHS for 24 h, and that there was a concentration-dependent diminution in the cytoplasm of AGS cells, with a progressive augmentation in the nuclei of AGS cells (Fig. 7A and B). After that, Immunofluorescence confocal showed, Nrf2 is obviously augmentation in cellular nucleus with NaHS (50 μM) treatment for 24 h compared with Vehicle treatment. (Fig. 7C). We further examined the relationship between H_2S and Nrf2 activity by transfection of DNA constructs containing a Nrf2 promoter region into AGS cells. As shown luciferase reporter assay, H_2S significantly augmented Nrf2 promoter luciferase activity in AGS cells with NaHS (50 μM) treatment for 24 h (Fig. 7D). ChIP assay further revealed that H_2S promoted interaction between Nrf2 and its target gene CD36 in AGS cells with NaHS (50 μM) treatment for 24 h (Fig. 7E). To test whether the H_2S promoted Nrf2 nuclear translocation and up-regulated gene expression levels of CD36, we examined the impact on LC-FA uptake and migration of treating AGS cells with siRNA to Nrf2. We found that Nrf2 knockdown also decreased the promote effect on cellular LC-FA uptake and migration with NaHS (50 μM) treatment for 24 h (Fig. 7A, F and G). Therefore, the aforementioned results showed that H_2S up-regulated protein expression levels of CD36 by induced Nrf2 nuclear translocation.

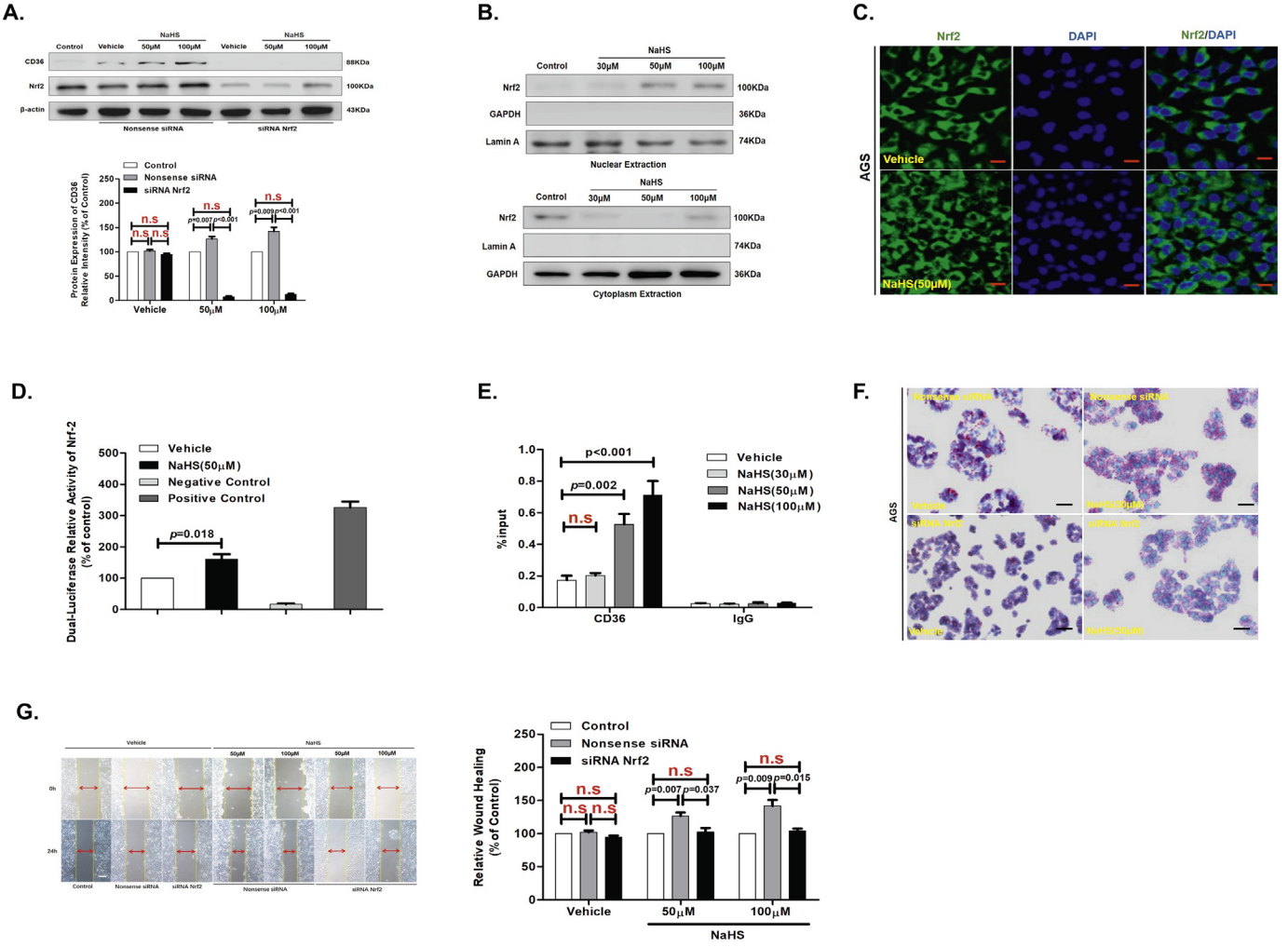

Fig. 7. H_2S up-regulated protein expression levels of CD36 *via* promoted Nrf2 nuclear translocation. (A) Western blots showing CD36 and Nrf2 protein levels in AGS cells (n = 3, student's t-test). (B) Western blot assay of Nrf2 from nuclear and cytoplasmic extracts of AGS cells treated with various concentrations of NaHS for 24 h. Combination of Lamin A and GAPDH was used as a loading control. (C) Immunofluorescence staining of Nrf2 in AGS cells after 24 h treatment with NaHS (50 μM). (D) Luciferase reporter assay measuring Nrf2 activity in AGC cells transiently co-transfected with pNrf2-Luc with NaHS treatment for 24 h at 50 μM (n = 3, student's t-test). (E) AGS cells were incubated with various concentrations of NaHS for 24 h and analyzed by a quantitative ChIP assay with anti-Nrf2 antibody (n = 3, student's t-test). (F) The promote effect of H_2S on cellular lipid uptake in the knockdown of Nrf2 in AGS cells by Oil Red O staining. (G) The promote effect of H_2S on cell migration in the knockdown of Nrf2 in AGS cells (n = 3, student's t-test). n.s, no significant differences. Each bar represents the mean ± standard deviation (S.D.).

4. Discussion

The LC-FA uptake capacity of adipocytes is thought to be mediated by CD36 following entrance 1 [32]. Here, we showed that CD36 can directly activate LC-FA access to the cytoplasm by acting as a direct target molecule for H_2S. Specifically, we identified a disulfide bond between Cys333 and Cys272 in the CD36 protein structure. The function of this disulfide bond in CD36 had not been reported to date (Fig. 8 and Fig. S4E).

The mechanisms underlying the interaction between H_2S and its target molecule may be different from that of a typical ligand-receptor interaction where the ligand docks in the binding pocket/cavity within its receptor. In fact, H_2S is too small a molecule to dock in any potential pockets/cavities *via* conformational matching. This idea was supported by our MS experiments as well as our theoretical analysis of quantum chemistry, where we identified the HS^- anion as the reactive nucleophile that breaks the Cys333-Cys272 disulfide bond within CD36. In neutral solutions, two-thirds of the HS^- anions dissociated from NaHS are transformed into H_2S, while the rest remain as HS^- anions [6].

In our previous studies, we observed significant effects at low concentrations of NaHS, where 30 μM, 50 μM, and 100 μM NaHS yielded H_2S concentrations of 20 μM, 30 μM, and 60 μM, respectively. It has been reported that plasma or blood sulfide concentrations range typically between 30 μM and 300 μM, indicating that the NaHS concentrations we used in the present study yielded physiologically relevant levels of H_2S in solution [44]. In addition, our previous studies compared the effects of NaHS and H_2S gas and revealed similar promoting effects on migration of vascular endothelial cells. We also examined the possible role of the oxidation products of NaHS. We identified three oxidation products in NaHS (50 μM) using ion chromatography, namely, SO_4^{2-} SO_3^{2-} and $S_2O_3^{2-}$. We then examined the migration-promoting effects of these oxidation products at different doses and found that none of them had any enhancing effect on cell migration at any concentration. These results suggested that the oxidation products of NaHS did not contribute to the effects observed in our *in vitro* and *in vivo* experiments [6].

In this study, we illustrated that GC cell lines show wide variations in their metabolic phenotypes. Interestingly, the subgroup of $CD36^{low}$ GC cell lines showed a low metabolic index. Several prior studies have demonstrated that H_2S donors can stimulate mitochondrial electron transport and ATP generation in various cell lines [45–48]. Furthermore, H_2S, *via* sulfhydration, has been shown to increase the catalytic activity of the glycolytic enzyme GAPDH [49]. Since tumor proliferation, migration, and invasion are energetically demanding processes, we speculate that inhibiting or silencing CD36 would contribute to energy starvation of the cancer cells and impair their metastasis [50]. The basal protein expression level of CD36 is low, and we overexpressing with the mutated Cys333 in AGS, CD36(C333A) expresses far more than CD36(wt) basal expression. We have performed a set of new experiments using PA to stimulate the AGS cells transfected with vectors over expressing mutant CD36(C333A) and using H_2S to stimulate the AGS cells transfected with vectors over expressing wild type CD36. The results showed that PA but

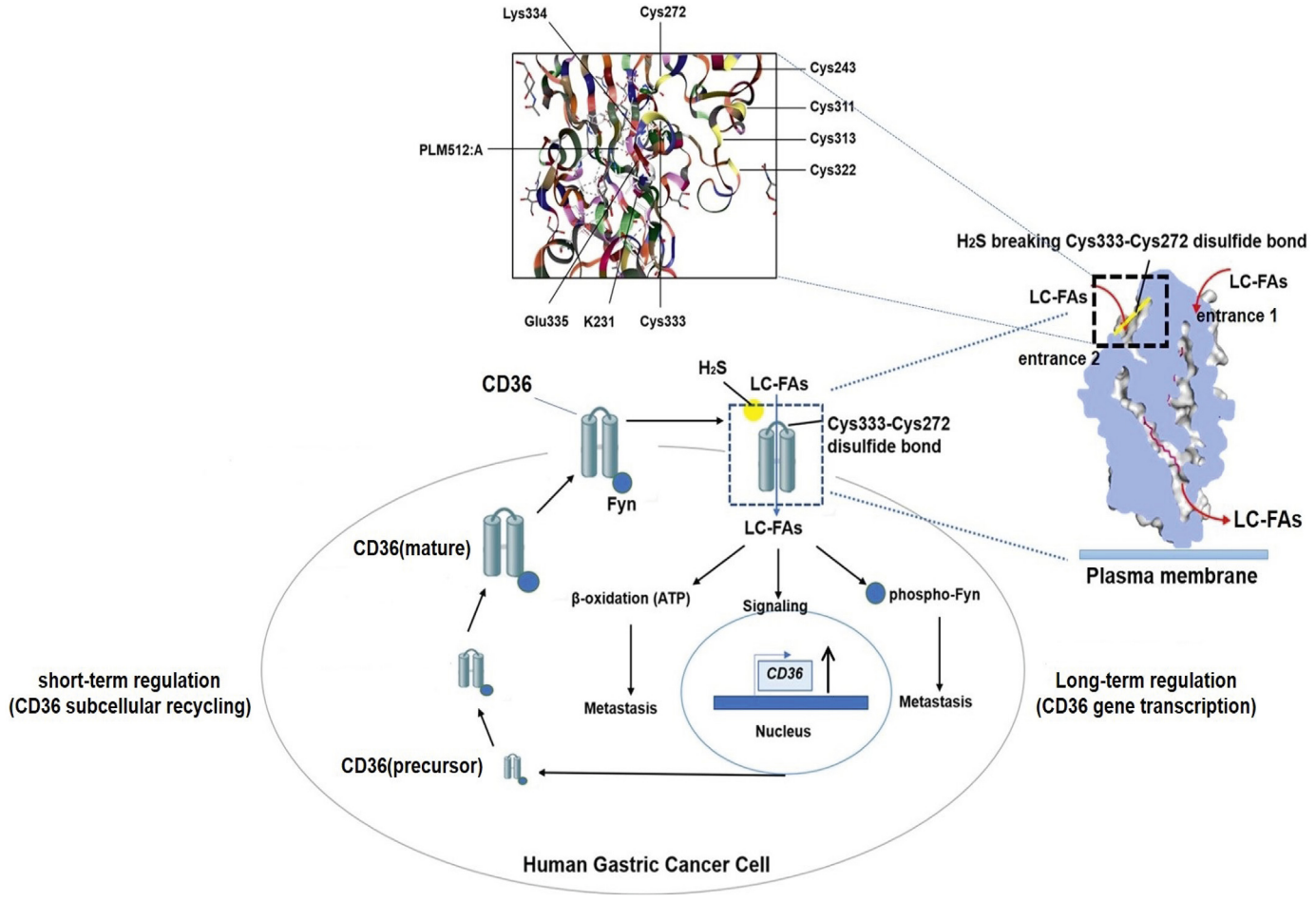

Fig. 8. Fatty-acid receptor CD36 functions as a hydrogen sulfide-targeting receptor with its Cys333-Cys272 disulfide bond serving as a specific molecular switch to accelerate gastric cancer metastasis. A schematic illustration of our systems-biology approach. We identified that CD36 functions as a H_2S-targeted receptor, with its Cys333-Cys272 disulfide bond serving as a specific molecular switch to accelerate human GC metastasis. Short-term regulation (CD36 subcellular recycling) and long-term regulation (CD36 gene transcription) form a positive feedback loop, with the Cys333-Cys272 disulfide bond within CD36 acting as a special molecular switch for this positive feedback. H_2S turns on this "switch" and induces LC-FA signaling, thus accelerating the metastasis of GC.

not H_2S further promoted the migration of transfected cells with mutant CD36(C333A), while H_2S could promoted the migration of transfected cells with wild type CD36. The data further illustrated that transfection of the cells with CD36(C333A) did not induce the maximal rate of the migration of these cells and Cys333-Cys272 of CD36 was probably the target site of H_2S. Therefore, the basal level of CD36(wt) did not interfering with the mutated Cys333 when transfected in the GC cells.

According to previous literature [51], CD36 inhibits angiogenesis in human microvascular endothelial cells (HMVECs). However, in tumor cells, there may be multiple signal pathway mutations. In particular, spleen tyrosine kinase (Syk) (as a non-receptor tyrosine kinase) plays a crucial role in signaling pathways downstream of CD36 that inhibit angiogenesis. Unfortunately, due to its high methylation levels in most of the GC cell lines [52,53], also including other types of cancer cells, Syk is absent (Fig. S4A). To test for the dephosphorylation of Fyn *via* the association of Syk with the CD36 interaction, we examined the impact on the migration of AGC cells stably expressing Syk. Surprisingly, we discovered that Syk overexpression noticeably decreased the promotion effect on AGS cell migration with NaHS (50 μM) treatment, and NaHS (50 μM) cannot phosphorylate Fyn at the 530 site *via* CD36, even though CD36 is not a tyrosine kinase receptor (Fig. S4B-S4D). In addition, it has been reported that CD36 promotes VEGF release in various types of cancer cell lines [54–56]. Therefore, these results suggested that H_2S promoted the release of VEGF *via* CD36 in AGC cells.

In summary, efforts toward finding effective inhibitors of metastasis have not been very successful, primarily due to drug ineffectiveness, the presence of adverse reactions, and the development of drug resistance. Genetic and pharmacological blockade of CD36 function could be harnessed as an anti-metastasis therapeutic strategy. Our study provides new insights for a better understanding of the molecular mechanisms of H_2S in cancer metastasis.

Acknowledgments

We thank Dr. Yong Huang and Dr. Yadan Bai for their technical supports, and Dr. Zhendong Xiang and Dr. Guangxue Wang for their support on animal modeling and animal study. We thank Prof. Xianhua Sun and members of Tongji hospital central laboratory affiliated to Tongji university for their helps throughout the study.

Author contributions

RW designed research plan, conducted the experiments, analyzed all data, and wrote the manuscript. LC, SW, QF, JZ conducted the mice experimentation. ZW, SD, WW, YH assisted with some experiments. YC, TL, SB, XW, XQ, KW, XM and YK collaborated to collect endoscopy biopsies. BT and ZW supervised the experimental work and data analyses. All authors participated in revising the manuscript and agreed to the final version.

Funding source

This study was supported by grants from Strategic Priority Research Program of the Science and Technology Commission of Shanghai (1312JC1408402, Recipient: ZRW). The founding source had no involvements in study design, data collection, data analysis, data interpretation, manuscript preparation and submission.

Disclosure of potential conflicts of interest

All authors have no potential conflicts of interest.

Ethical standards

The authors have no ethical conflicts to disclose.

Conflict of interest

The authors declare no potential conflicts of interest.

Appendix A. Supplementary data

Supplementary data to this article can be found online at https://doi.org/10.1016/j.ebiom.2019.06.037.

References

[1] Wang R. Physiological implications of hydrogen sulfide: a whiff exploration that blossomed. Physiol Rev 2012;92:791–896.
[2] Wang R. Hydrogen sulfide: the third gasotransmitter in biology and medicine. Antioxid Redox Signal 2010;12:1061–4.
[3] Bian JS, Olson KR, Zhu YC. Hydrogen sulfide: biogenesis, physiology, and pathology. Oxid Med Cell Longev 2016;2016:1–2.
[4] Zhao H, Alam A, Soo AP, George AJT, Ma D. Ischemia-reperfusion injury reduces long term renal graft survival: mechanism and beyond. EbioMedicine 2018;28:31–42.
[5] Cai WJ, Wang MJ, Moore PK, Jin HM, Yao T, Zhu YC. The novel proangiogenic effect of hydrogen sulfide is dependent on Akt phosphorylation. Cardiovasc Res 2007;76:29–40.
[6] Tao BB, Liu SY, Zhang CC, Fu W, Cai WJ, Wang Y, et al. VEGFR2 functions as an H_2S-targeting receptor protein kinase with its novel Cys1045-Cys1024 disulfide bond serving as a specific molecular switch for hydrogen sulfide actions in vascular endothelial cells. Antioxid Redox Signal 2013;19:448–64.
[7] Ge SN, Zhao MM, Wu DD, Chen Y, Wang Y, Zhu JH, et al. Hydrogen sulfide targets EGFR Cys797/Cys798 residues to induce Na(+)/K(+)-ATPase endocytosis and inhibition in renal tubular epithelial cells and increase sodium excretion in chronic salt-loaded rats. Antioxid Redox Signal 2014;21:2061.
[8] Ma SF, Luo Y, Ding YJ, Chen Y, Pu SX, Wu HJ, et al. Hydrogen sulfide targets the Cys320/Cys529 motif in Kv4.2 to inhibit the ito potassium channels in cardiomyocytes and regularizes fatal arrhythmia in myocardial infarction. Antioxid Redox Signal 2015;23:129.
[9] Yang G, Wu L, Jiang B, Yang B, Qi J, Cao K, et al. H_2S as a physiologic vasorelaxant: hypertension in mice with deletion of cystathionine γ-lyase. Science 2008;322:587–90.
[10] Tao BB, Wang R, Sun C, Zhu YC. 3-mercaptopyruvate sulfurtransferase, not cystathionine β-synthase nor cystathionine γ-lyase, mediates hypoxia-induced migration of vascular endothelial cells. Front Pharmacol 2017;8:657.
[11] Zhou YF, Wu XM, Zhou G, Mu MD, Zhang FL, Li FM. Cystathionine β-synthase is required for body iron homeostasis. Hepatology 2017;67.
[12] Wang R, Fan Q, Zhang J, Zhang X, Kang Y, Wang Z. Hydrogen sulfide demonstrates promising antitumor efficacy in gastric carcinoma by targeting MGAT5. Transl Oncol 2018;11:900–10.
[13] Szabo C, Coletta C, Chao C, Módisa K, Szczesnyc B, Papapetropoulosa A, et al. Tumor-derived hydrogen sulfide, produced by cystathionine-β-synthase, stimulates bioenergetics, cell proliferation, and angiogenesis in colon cancer. Proc Natl Acad Sci U S A 2013;110:12474–9.
[14] Phillips CM, Zatarain J, Nicholls ME, Porter C, Steve GW, Thanki K. Up-regulation of cystathionine-β-synthase in colonic epithelia reprograms metabolism and promotes carcinogenesis. Cancer Res 2017;3480:2017.
[15] Vander Heiden MG, Cantley LC, Thompson CB. Understanding the Warburg effect: the metabolic requirements of cell proliferation. Science 2009;324:1029–33.
[16] Zhang MM, di Martino Julie S, Robert LB, Nathaniel RC, Baksh Sanjeethan C, Simon-Vermot Theresa, et al. Adipocyte-derived lipids mediate melanoma progression via FATP proteins. Cancer Discov 2018;14 [CD-17-1371].
[17] Hsieh FL, Turner L, Bolla JR, Robinson CV, Lavstsen T, Higgins MK. The structural basis for CD36 binding by the malaria parasite. Nat Commun 2016;7:12837.
[18] Pascual G, Avgustinova A, Mejetta S, Martin M, Castellanos A, Attolini CS, et al. Targeting metastasis-initiating cells through the fatty acid receptor CD36. Nature 2017;541:41–5.
[19] Nieman KM, Kenny HA, Penicka CV, Latanya A, Buell-Gutbrod R, Zillhardt MR, et al. Adipocytes promote ovarian cancer metastasis and provide energy for rapid tumor growth. Nat Med 2011;17:1498.
[20] Ladanyi A, Mukherjee A, Kenny HA, Johnson A, Mitra AK, Sundaresan S, et al. Adipocyte-induced CD36 expression drives ovarian cancer progression and metastasis. Oncogene 2018;37:2285–301.
[21] Osman MA, Hennessy BT. Obesity correlation with metastases development and response to first-line metastatic chemotherapy in breast cancer. Clin Med Insights Oncol 2015;9:105–12.
[22] Hale JS, Otvos B, Sinyuk M, Alvarado AG, Hitomi M, Stoltz K, et al. Cancer stem cell-specific scavenger receptor CD36 drives glioblastoma progression. Stem Cells 2014;32:1746–58.
[23] Yu L, Han H, Liu LP, Duan YJ, Yang XX, Ma CR, et al. CD36 plays a critical role in proliferation, migration and tamoxifen-inhibited growth of ER-positive breast cancer cells. Oncogenesis 2018;7:98.
[24] Jia S, Zhou L, Shen T, Zhou SH, Ding GP, Cao LP. Down-expression of CD36 in pancreatic adenocarcinoma and its correlation with clinicopathological features and prognosis. J Cancer 2018;9:578–83.
[25] Watt MJ, Clark AK, Selth LA, Haynes VR, Lister N, Rebello R, et al. Suppressing fatty acid uptake has therapeutic effects in preclinical models of prostate cancer. Sci Transl Med 2019;11.

[26] Hawk MA, Schafer ZT. Mechanisms of redox metabolism and cancer cell survival during extracellular matrix detachment. J Biol Chem 2018;293:7531–7.
[27] Marsboom G, Rehman J. Redox and metabolic regulation of transcription. Oncotarget 2016;7:80107–8.
[28] Fan Z, Wirth AK, Chen D, Wruck CJ, Rauh M, Buchfelder M, et al. Nrf2-Keap1 pathway promotes cell proliferation and diminishes ferroptosis. Oncogenesis 2017;6:e371.
[29] Cloer EW, Goldfarb D, Schrank TP, Weissman BV, Major MB. Nrf2 Activation in Cancer: From DNA to Protein. Cancer Res 2019;79:889–98.
[30] Pan J, Fan Z, Wang Z, Dai Q, Xiang Z, Yuan F, et al. CD36 mediates palmitate acid-induced metastasis of gastric cancer via AKT/GSK-3β/β-catenin pathway. J Exp Clin Cancer Res 2019;38:52.
[31] Tan Y, Lin K, Zhao Y, Wu Q, Chen D, Wang J, et al. Adipocytes fuel gastric cancer omental metastasis via PITPNC1-mediated fatty acid metabolic reprogramming. Theranostics 2018;8:5452–68.
[32] Neculai D, Schwake M, Ravichandran M, Zunke F, Collins RF, Peters J. Structure of limp-2 provides functional insights with implications for SR-BI and CD36. Nature 2013;504:172–6.
[33] Kuda O, Pietka TA, Demianova Z, Kudova E, Cvacka J, Kopecky J, et al. Sulfo-n-succinimidyl oleate (SSO) inhibits fatty acid uptake and signaling for intracellular calcium via binding CD36 lysine 164. SSO also inhibits oxldl uptake by macrophages. J Biol Chem 2013;288:15547–55.
[34] Kashihara H, Shimada M, Yoshikawa K, Higashijima J, Tokunaga T, Nishi M, et al. Correlation between thrombospondin-1 expression in non-cancer tissue and gastric carcinogenesis. Anticancer Res 2017;37:3547–52.
[35] Hamilton JA, Kamp F. How are free fatty acids transported in membranes? Is it by proteins or by free diffusion through the lipids? Diabetes 1999;48:2255–69.
[36] Bergers G, Hanahan D. Modes of resistance to anti-angiogenic therapy. Nat Rev Cancer 2008;8:592–603.
[37] Cao Y. Angiogenesis modulates adipogenesis and obesity. J Clin Invest 2017;117:2362–8.
[38] Iwamoto H, Abe M, Yang Y, Cui D, Seki T, Nakamura M. Cancer lipid metabolism confers antiangiogenic drug resistance. Cell Metab 2018;28:1.
[39] Kuhajda FP. Fatty acid synthase and cancer: new application of an old pathway. Cancer Res 2006;66:5977–80.
[40] Cai W, Wang M, Ju L, Wang C, Zhu Y. Hydrogen sulfide induces human colon cancer cell proliferation: role of Akt, ERK and p21. Cell Biol Int 2010;34:565–72.
[41] Hosoki R, Matsuki N, Kimura H. The possible role of hydrogen sulfide as an endogenous smooth muscle relaxant in synergy with nitric oxide. Biochem Biophys Res Commun 1997;237:527–31.
[42] Chio IC, Jafarnejad SM, Ponzsarvise M, Park Y, Rivera K, Palm W, et al. Nrf2 promotes tumor maintenance by modulating mRNA translation in pancreatic cancer. Cell 2016;4:963–76.
[43] Hourihan JM, Kenna JG, Hayes JD. The gasotransmitter hydrogen sulfide induces Nrf-2-target genes by inactivating the Keap-1 ubiquitin ligase substrate adaptor through formation of a disulfide bond between Cys226 and Cys613. Antioxid Redox Signal 2013;19:465–81.
[44] Abe K, Kimura H. The possible role of hydrogen sulfide as an endogenous neuromodulator. J Neurosci 1996;16:1066–71.
[45] Szabo C, Céline R, Katalin M, Andriamihaja M, Murghes B, Coletta C, et al. Regulation of mitochondrial bioenergetic function by hydrogen sulfide. Part I. Biochemical and physiological mechanisms. Br J Pharmacol 2014;171:2099–122.
[46] Bian JS, Yong QC, Pan TT, Feng ZN, My Ali, Zhou S, et al. Role of hydrogen sulfide in the cardio protection caused by ischemic preconditioning in the rat heart and cardiac myocytes. J Pharmacol Exp Ther 2006;316:670–8.
[47] Liu Y, Zuckier LS, Ghesani NV. Dominant uptake of fatty acid over glucose by prostate cells: a potential new diagnostic and therapeutic approach. Anticancer Res 2010;30:369–74.
[48] Cao Y. Adipose tissue angiogenesis as a therapeutic target for obesity and metabolic diseases. Nat Rev Drug Discov 2010;9:107–15.
[49] Mir S, Sen T, Sen N. Cytokine-induced GAPDH sulfhydration affects PSD95 degradation and memory. Mol Cell 2014;56:786–95.
[50] Enciu AM, Radu E, Popescu ID, Hinescu ME, Ceafalan LC. Targeting CD36 as biomarker for metastasis prognostic: how far from translation into clinical practice? Biomed Res Int 2018;2018:1–12.
[51] Chu LY, Ramakrishnan DP, Silverstein RL. Thrombospondin-1 modulates VEGF signaling via CD36 by recruiting SHP-1 to VEGFR2 complex in microvascular endothelial cells. Blood 2013;122:1822–32.
[52] Chakraborty G, Rangaswami H, Jain S, kundu GC. Hypoxia regulates cross-talk between Syk and Lck leading to breast cancer progression and angiogenesis. J Biol Chem 2006;281:11322–31.
[53] Chuanliang P, Yunpeng Z, Yingtao H, Qifeng S, Xiaogang Z, Bo C. Syk expression in non-small-cell lung cancer and its relation with angiogenesis. J Cancer Res Ther 2016;12:663.
[54] Kaur B, Cork SM, Sandberg EM, Devi NS, Zhang Z, Klenotic PA, et al. Vasculostatin inhibits intracranial glioma growth and negatively regulates in vivo angiogenesis through a CD36-dependent mechanism. Cancer Res 2009;69:1212–20.
[55] Zingg JM, Azzi A, Meydani M. α-Tocopheryl phosphate induces VEGF expression via CD36/PI3Kγ in THP-1 monocytes. J Cell Biochem 2017;118:1855.
[56] Sp N, Kang DY, Kim DH, Park JH, Lee HG, Kim HJ, et al. Nobiletin inhibits CD36-dependent tumor angiogenesis, migration, invasion, and sphere formation through the Cd36/Stat3/Nf-Kb signaling axis. Nutrients 2018;10:772.